40 CFR Part 191
Subparts B and C
Compliance Recertification Application 2026
for the
Waste Isolation Pilot Plant

Appendix HYDRO-2026
Hydrological Investigations

United States Department of Energy
Waste Isolation Pilot Plant

Carlsbad Field Office
Carlsbad, New Mexico

Compliance Recertification Application 2026
Appendix HYDRO-202

TABLE OF CONTENTS

HYDRO-1.0 HYDROLOGICAL STUDIES 1

HYDRO-2.0 HYDRAULIC TESTING 4

HYDRO-3.0 GEOCHEMICAL DATA ACQUISITION AND ANALYSES 10

HYDRO-4.0 GEOLOGICAL INFORMATION 17

HYDRO-5.0 WELL REPLACEMENT 19

HYDRO-6.0 MONITORING 20
- HYDRO-6.1 Culebra Monitoring 20
- HYDRO-6.2 Normalized Hydrograph 23
- HYDRO-6.2 Magenta Monitoring 31
- HYDRO-6.3 Dewey Lake Monitoring 34
- HYDRO-6.4 Bell Canyon Monitoring 35

HYDRO-7.0 CULEBRA GROUND WATER FLOW DIRECTION 36

HYDRO-8.0 SUMMARY 40

HYDRO-9.0 REFERENCES 40

LIST OF TABLES

Table HYDRO-1. Geology at Borehole C-3977 (Pre-Shaft Core hole) modified from Powers et al. (2018). 18
Table HYDRO-2. Wells Plugged and Abandoned 2018—2022 19

LIST OF FIGURES

Figure HYDRO-1. Locations of WIPP Wells. The Land Withdrawal Boundary (LWB) is indicated by a Grey Line. Wells Inside the Land Withdrawal Area (LWA) are shown in an Inset to better differentiate Well Locations. Note that C-2737 is a Dual Completion Well in Both the Culebra and Magenta. 2
Figure HYDRO-2. General Stratigraphic Column of Geologic Units at the WIPP Site modified from CRA-2009. 3
Figure HYDRO-3. The Flow Dimension Diagnostic for Culebra wells WIPP-11 (green X) and WIPP-11R (red circles) and 100 Model Fits to the WIPP-11R Flow Dimension Diagnostic Data (blue lines). 5
Figure HYDRO-4. Spatial Distribution of the Logarithm of Culebra Hydraulic Conductivity Surrounding Well WIPP-11, (a) Initial $log_{10}\ K$ and (b) the $log_{10}\ K$ Resulting from Recalibration using the Bourdet Pressure Change Diagnostic. 7
Figure HYDRO-5. Histogram of the Root Mean Square Errors (RMSEs) between Simulated and Observed Hydraulic Heads. RMSEs are Shown for the Initial and Calibrated T-field Realizations. 8
Figure HYDRO-6. Average Transmissivity Across Initial (a) and Calibrated (b) Realizations 9
Figure HYDRO-7. The Average Cation/Anion Concentrations for Predominant Analytes Sampled in Culebra WIPP Monitoring Wells with Respect to Longitude (A) and Latitude (B). 11
Figure HYDRO-8. Update of Culebra Hydrogeochemical Facies A from Siegel et al. (1991) 15
Figure HYDRO-9. Updated Culebra Hydrogeochemical Facies (Kirkes et al. 2022). The Green Area Denotes Cation Exchange Between Na^+ and Ca^{2+}. Note that the well labeled SNL-17 is well SNL-17a. 16
Figure HYDRO-10. Piper Diagram of Samples from the Culebra Well Network (Kirkes et al. 2022) 17
Figure HYDRO-11. Depth to Water Measurements and Pressure Transducer Data for Well C-2737. 21
Figure HYDRO-12. Culebra Well Locations and Their Hydrograph Groupings 22
Figure HYDRO-13. A Hydrograph of Normalized Head for All Current WIPP Monitoring Network Wells Screened for Anthropogenic Effects (modified from Bowman 2025). 24
Figure HYDRO-14. Water Level Elevations for Culebra Wells Impacted by Shaft Leakage 24
Figure HYDRO-15. Water Level Elevations for Northern Culebra Wells #1 25

Figure HYDRO-16. Water Level Elevations for Northern Culebra Wells #2 26
Figure HYDRO-17. Water Level Elevations and Rainfall Data for Culebra Wells Near Nash Draw with Rainfall Data. 27
Figure HYDRO-18. Water Level Elevations for Culebra Long-Term Recovery Wells 28
Figure HYDRO-19. Water Level Elevations for Culebra Plugged and Abandoned Wells 29
Figure HYDRO-20. Wells with Anthropogenically Affected Water Level Elevations in Close Proximity to Well C-02348. 30
Figure HYDRO-21. Wells with Anthropogenically Affected Water Level Elevations 31
Figure HYDRO-22. Water Level Elevation in Magenta Wells Inside the LWB 33
Figure HYDRO-23. Water Level Elevation in Magenta Wells Outside the LWB 34
Figure HYDRO-24. Dewey Lake Water Levels 35
Figure HYDRO-25. Bell Canyon Water Levels 36
Figure HYDRO-26. 2013 Simulated Freshwater Head Contours (5-foot Contour Interval). The Dashed Line Represents the DTRKMF Simulated Particle Pathway from the Waste Handling Shaft to the WIPP LWB (Travel Time = 6,234 Years) (DOE 2014). 37
Figure HYDRO-27. 2023 Simulated Freshwater Head Contours (5-foot Contour Interval). The Dashed Line Represents the DTRKMF Simulated Particle Pathway from the Waste Handling Shaft to the WIPP LWB (Travel Time = 6,583 Years). 38
Figure HYDRO-28. Simulated Freshwater Head Contours for 2013 and 2023. From 2013 to 2023, there is a Decrease in Simulated Heads and a Westward Shift in Particle Path. These Changes are Due to a) the Use of New Calibrated Parameter Fields (Bowman et al. 2023) in 2023 and b) the Impact of Shaft 5 Mining on Culebra Water Levels. 39

ACRONYMS AND ABBREVIATIONS

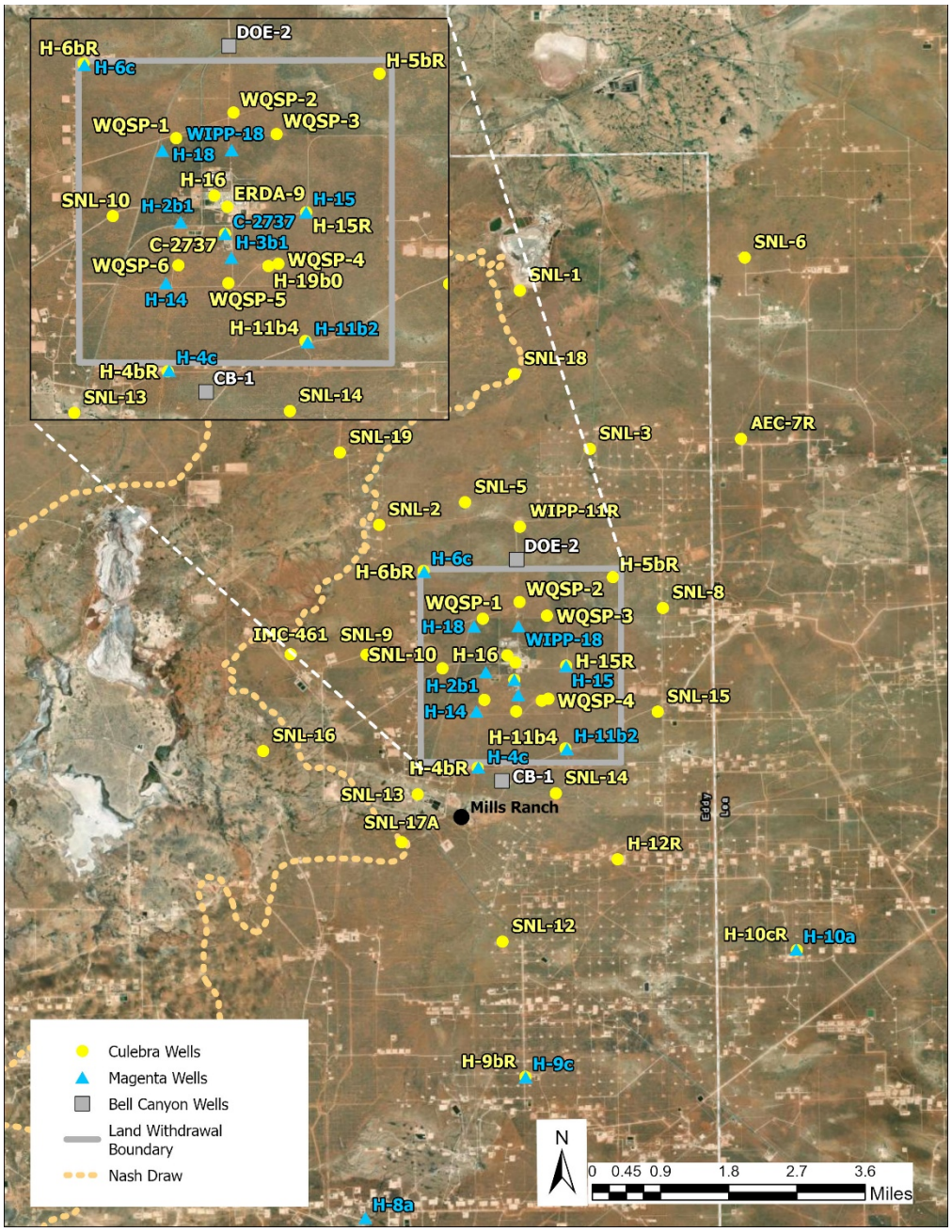
AF	acre-feet
AMSL	above mean sea level
AP	analysis plan
ASER	Annual Site Environmental Report
CB	Cabin Baby
cm	centimeter
CRA	Compliance Recertification Application
DOE	U.S. Department of Energy
EPA	U.S. Environmental Protection Agency
LWB	Land Withdrawal Boundary
m	meter
m^2/s	square meters per second
min	minute
NOAA	National Oceanic and Atmospheric Administration
PA	performance assessment
P&A	plugged and abandoned
R	Replacement
SNL	Sandia National Laboratories
SP	Specific Procedure
TP	test plan
T	transmissivity
WIPP	Waste Isolation Pilot Plant

HYDRO-1.0 HYDROLOGICAL STUDIES

This appendix summarizes hydrologic information for the Waste Isolation Pilot Plant (WIPP) that has been collected, analyzed, or incorporated since the January 8, 2018 data cutoff for the 2019 Compliance Recertification Application (CRA-2019). This summary is provided pursuant to the requirements of 40 CFR § 194.15 (U.S. EPA 1996). Over that period, additional hydrologic information related to the magnitude and direction of ground water flow and ground water quality was generated through DOE sponsored research and monitoring programs.

The material is presented in the following sections, which summarize key hydrologic analyses, monitoring results, and geological updates. Appendix HYDRO-2.0 summarizes hydraulic pumping and slug test analyses conducted on wells in the WIPP monitoring network and the modeling performed to better characterize non-radial flow in the Culebra Dolomite Member of the Rustler Formation, hereafter the Culebra. Many groundwater models assume radial flow around pumping or injection points. However, flow in the Culebra is strongly influenced by heterogeneities (e.g. fractures and variable transmissivity zones). These features can produce preferential flow paths that can deviate significantly from radial behavior, making non-radial flow directly relevant to long-term performance assessment at WIPP. Appendix HYDRO-3.0 presents the results of water quality monitoring and geochemical analyses of the Culebra groundwater samples. Monitoring groundwater quality and composition in the Culebra provides essential information on geochemical conditions that influence radionuclide mobility, sorption behavior, and transport pathways. This data help ensure that PA models accurately represent the chemical environment through which any contaminants could migrate. Appendix HYDRO-4.0 describes the new geologic information gathered since the January 8, 2018 data cutoff of CRA-2019. The coring and geotechnical characterization of borehole C-3977, a pre-Shaft #5 core hole, confirmed reference stratigraphy. Appendix HYDRO-5.0 describes the wells that were plugged and abandoned or replaced since the CRA-2019. Plugged and abandoned wells were phased out as part of the well optimization plan produced by Kuhlman (2010). Two wells were replaced, updating their casing from steel to fiberglass reinforced plastic. Appendix HYDRO-6.0 describes the water level monitoring performed since the CRA-2019 and the changes in water levels that have been observed. Historic and recent water level elevations are presented and discussed with hydrographs for WIPP monitoring network wells. Measurements from these wells support the calibration of flow models for PA and repository compliance. Appendix HYDRO-7.0 discusses the generation of piezometric surface maps using the Culebra groundwater model discussed in Appendix TFIELD-2014. Culebra flow directions are described with this analysis utilizing the data presented in Appendices HYDRO-4.0 and 6.0. Appendix HYDRO-8.0 provides an integration of all the new hydrological information collected since the CRA-2019.

For general reference, Figure HYDRO-1 presents a map of the locations of functional Culebra wells in the WIPP monitoring network relevant to this appendix. Figure HYDRO-2 provides the generalized stratigraphy surrounding the repository.



Imagery from: https://services.arcgisonline.com/ArcGIS/rest/services/World_Imagery/MapServer)

Figure HYDRO-1. Locations of WIPP Wells. The Land Withdrawal Boundary (LWB) is indicated by a Grey Line. Wells Inside the Land Withdrawal Area (LWA) are shown in an Inset to better differentiate Well Locations. Note that C-2737 is a Dual Completion Well in Both the Culebra and Magenta.

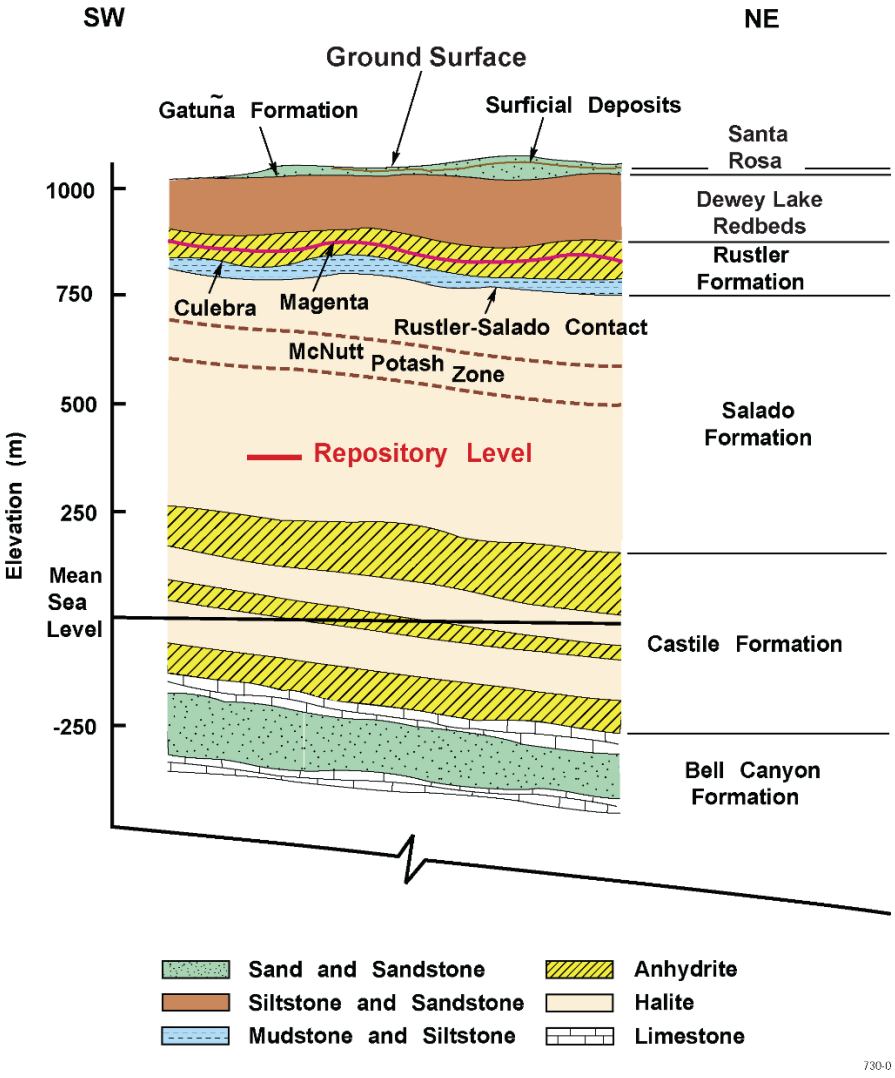


Figure HYDRO-2. General Stratigraphic Column of Geologic Units at the WIPP Site modified from CRA-2009.

HYDRO-2.0 HYDRAULIC TESTING

Hydraulic testing of groundwater wells at the WIPP is conducted under Test Plan (TP) 03-01 (Schuhen 2010), and interpretation of the resulting data follows Analysis Plan (AP)-070 (Bowman 2020b). Since CRA-2019, data from four tests conducted in the Culebra were analyzed to derive additional estimates of aquifer parameters: two new hydraulic tests and two tests prior to this CRA cycle. The resulting parameters were subsequently used in the recalibration of the transmissivity field (T-Field) used as input to the Culebra flow model. The T-fields comprise spatial distributions of transmissivity (*T*), storativity (*S*), hydraulic conductivity anisotropy ratio (*A*), and recharge rate (*R*) (Hart et al. 2009). Appendix HYDRO-2.0 discusses those hydraulic tests and their analyses.

Bowman (2014) summarized a constant-rate pumping test of well H-9bR, where "R" designates a replacement well by naming convention. This test was conducted in August 2012, during which a 3-acre-foot volume was pumped and water level responses recorded at six adjacent wells (H-4bR, H-7b1, SNL-12, SNL-14, SNL-17, and the Engle well, a nearby private well). Though the testing and analysis of this well was conducted prior to 2018, the results were not presented in CRA-2019 but are included here and were included in the calibration of T-fields. This test contrasted to the original test of well H-9b (Beauheim and Ruskoff 1998) in which the well was pumped for 8.8 days producing an ~0.4-acre-foot volume. Analysis of the pumping test yielded a geometric mean *T* of 1.45E-04 meters squared per second (m^2/s) and a mean *S* of 2.52E-06 where *T* was similar to that of the original H-9b test (9.8E-05 m^2/s) but a lower value compared to *S* (7.3E-04). The parameter estimates and adjusted freshwater heads derived from pressure heads measured in the observation wells were used in the calibration of CRA-2026 T-fields.

Bowman (2020a) summarized a constant-rate pumping test of well H-15R conducted in August 2008, during which 1,296 gallons were pumped, and water level response was recorded at the pumping well. Analysis of the test yielded a geometric mean *T* of 1.23E-07 m^2/s with *S* fixed at 8.10E-06. Transmissivities interpreted from these tests were used for single-well formation performance in the calibration of CRA-2026 T-fields.

Two tests were conducted in replacement wells for the originally steel-cased H-5b and WIPP-11. Bowman (2022a) summarized the analysis of a slug-withdrawal test conducted in December 2021 for well H-5bR. The estimated Culebra *T* had a geometric mean of 6.46E-08 m^2/s and mean *S* of 6.46E-08. These values differ from those of Dennehy and Mercer (1982) who used analysis of both a shut-in test and slug test to estimate a *T* of 2.1E-07 m^2/s and S of 1.0E-05. Bowman (2022b) summarized the analysis of a constant-rate pumping test conducted in September 2021 for well WIPP-11R. The estimated geometric mean of Culebra *T* for WIPP-11R was 7.59E-04 m^2/s with a mean *S* of 3.19E-06. The previous WIPP-11 test produced a geometric mean *T* of 4.27E-04 m^2/s and a mean *S* of 6.40E-06 (Roberts 2006). As part of the well test analysis, Bourdet derivatives (a representation of delta pressure and derivative of delta pressure) and flow dimension (a dimensionless representation of the second derivative of delta pressure) were calculated and modeled (Bourdet et al. 1989, Barker 1988). For uniform flow,

the Bourdet derivative typically settles to continuous constant values as flow approaches a steady state. Flow in heterogeneous media will result in deviations from continuous value which can be used to inform the proximity and degree of heterogeneity as flow propagates from a testing well. The WIPP-11 and WIPP-11R pressure derivatives and flow dimensions were of unique interest as the Bourdet diagnostic calculated from the WIPP-11 pumping test Culebra pressure data demonstrated a repeating sinusoidal flow-extent pattern (Roberts 2006). Although conducted at different times and in different wells on the same pad, the WIPP-11 and WIPP-11R tests display similar non-radial flow-dimension trends, although the WIPP-11 response was shifted in time relative to that observed in WIPP-11R (Figure HYDRO-3).

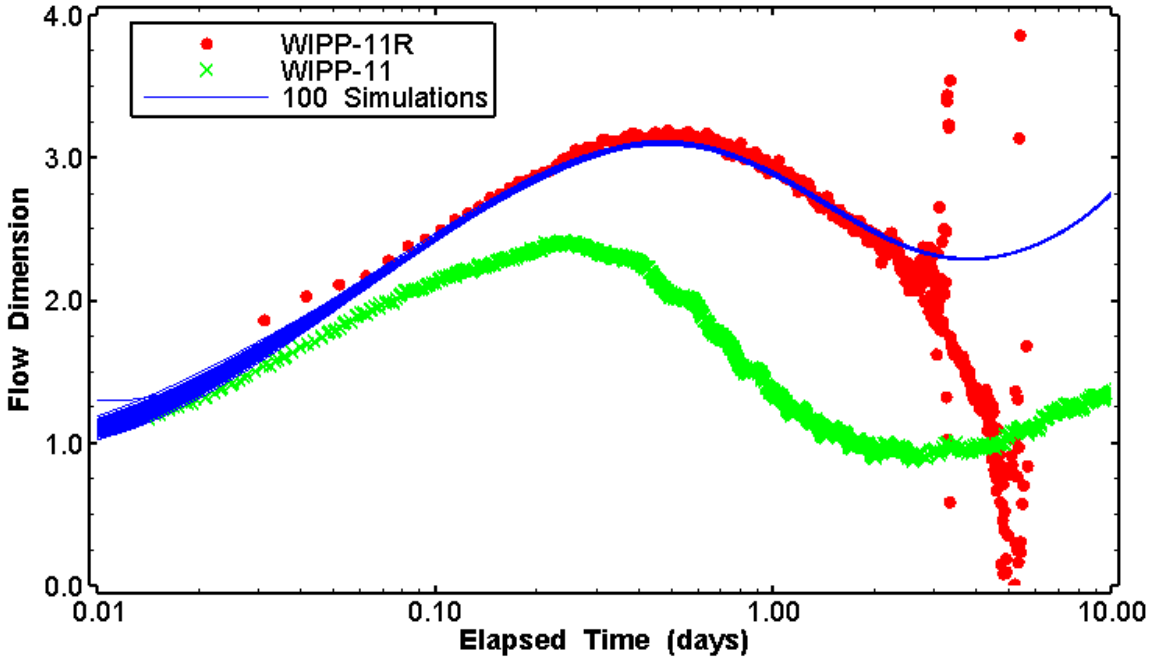


Figure HYDRO-3. The Flow Dimension Diagnostic for Culebra wells WIPP-11 (green X) and WIPP-11R (red circles) and 100 Model Fits to the WIPP-11R Flow Dimension Diagnostic Data (blue lines).

The repeatability of this non radial diagnostic highlighted limitations in earlier modeling assumptions and prompted renewed efforts to better characterize the more heterogeneous portions of the Culebra, particularly north and west of the WIPP LWB. Akara (2022) reanalyzed pumping tests for 12 Culebra wells using variable flow dimension and constant T models. Previous analyses (Beauheim and Roberts, 1998; Roberts 2006, 2007) assumed constant flow dimension and spatially variable T. Results indicate that 6 out of the 12 wells could be reanalyzed using the variable flow dimension approach, which produced new T values approximately one order of magnitude higher (P-14, SNL-2, SNL-5, and WIPP-11), or lower (SNL-9) than that of the previous analyses. Akara (2022) established that a spatially varying flow model was a reasonable approach but should only be used in combination with an improved characterization of heterogeneity. Based upon these initial results, Akara (2023) recalibrated

the CRA-2014 final T-fields using drawdown from WIPP-11 and five observation wells (SNL-3, H-6b, WIPP-13, WQSP-1, and WQSP-2). The pressure derivative of WIPP-11 recovery was also included as calibration target. Figure HYDRO-4 compares the spatial distribution of the logarithm of Culebra hydraulic conductivity ($log_{10}\ K$) surrounding well WIPP 11. Figure HYDRO-4a shows the initial $log_{10}\ K$ field prior to recalibration. Figure HYDRO-4b shows the recalibrated $log_{10}\ K$ field derived using a workflow that incorporates Bourdet pressure change diagnostics, which resulted in modifications to the spatial distribution of $log_{10}\ K$. The recalibrated hydraulic conductivity field shows that the time-variable flow-dimension observed at WIPP-11 may result from the presence of a NE-SW striking zone of high hydraulic conductivity bounded by a zone of lower $log_{10}\ K$.

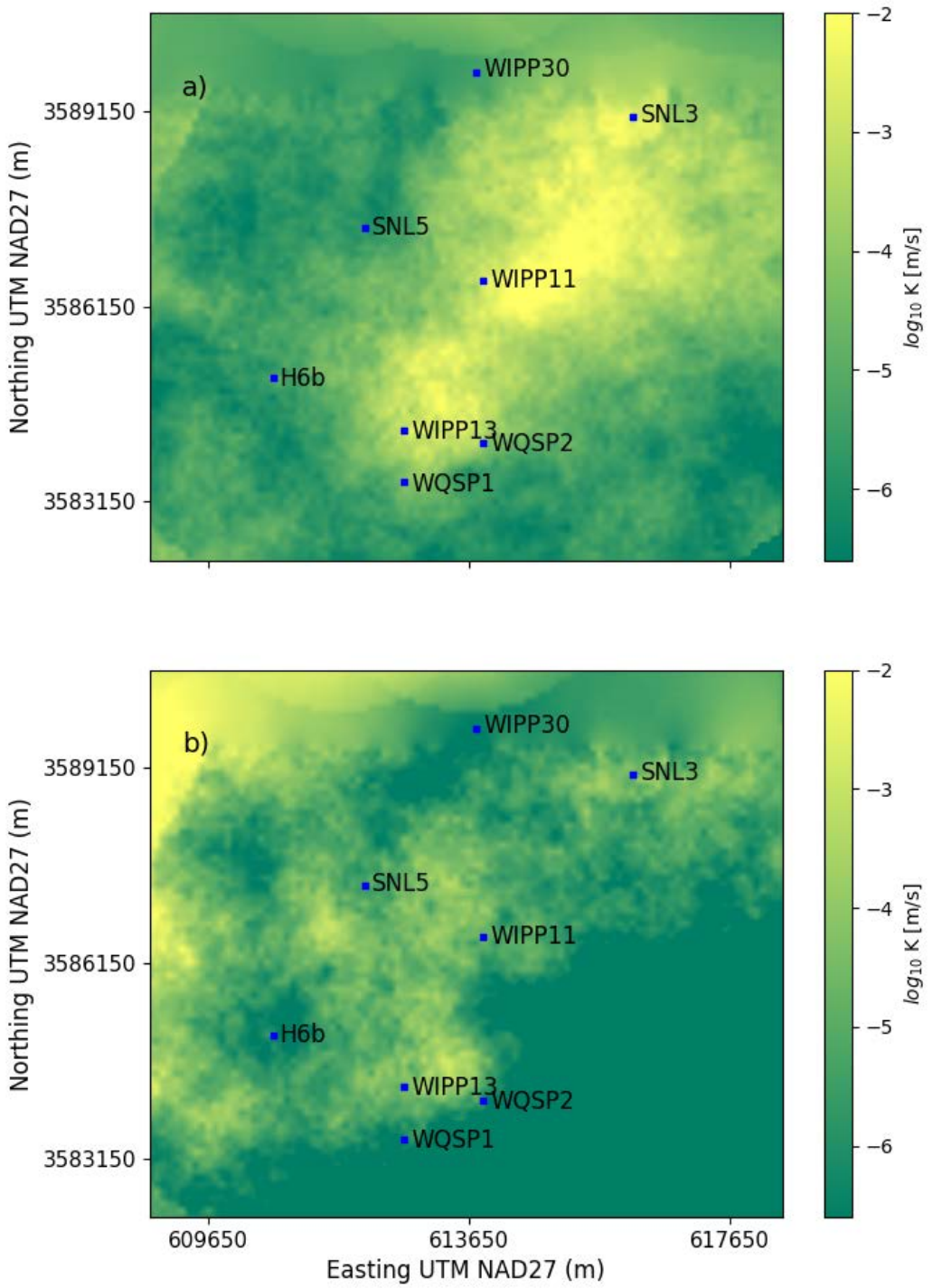


Figure HYDRO-4. Spatial Distribution of the Logarithm of Culebra Hydraulic Conductivity Surrounding Well WIPP-11, (a) Initial log_{10} *K* and (b) the log_{10} *K* Resulting from Recalibration using the Bourdet Pressure Change Diagnostic.

Using the same calibration approach, Akara (2024) recalibrated the final 100 T-fields, against drawdown and pressure derivative from 14 single-well pumping tests. Overall, the recalibrated T-fields produced lower root mean square errors between simulated and observed steady-state heads (Figure HYDRO-5). Figure HYDRO-6 shows the spatial changes in averaged transmissivity fields. These results suggest that pressure derivatives can be useful calibration targets for T-fields.

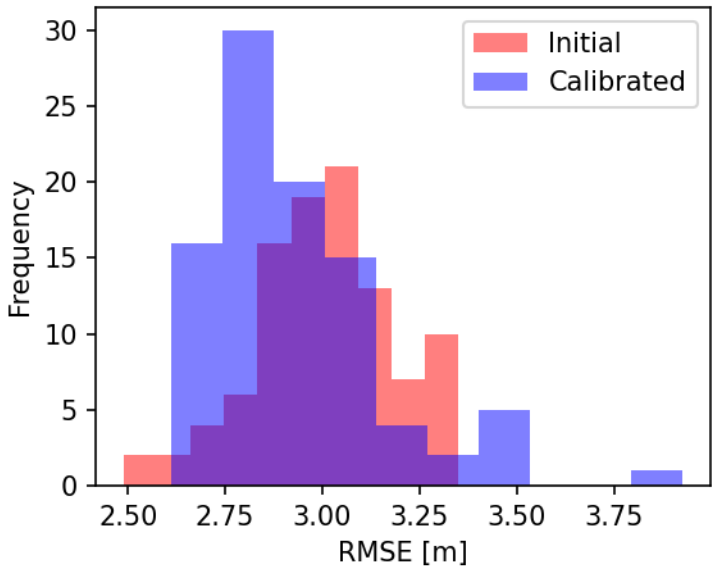


Figure HYDRO-5. Histogram of the Root Mean Square Errors (RMSEs) between Simulated and Observed Hydraulic Heads. RMSEs are Shown for the Initial and Calibrated T-field Realizations.

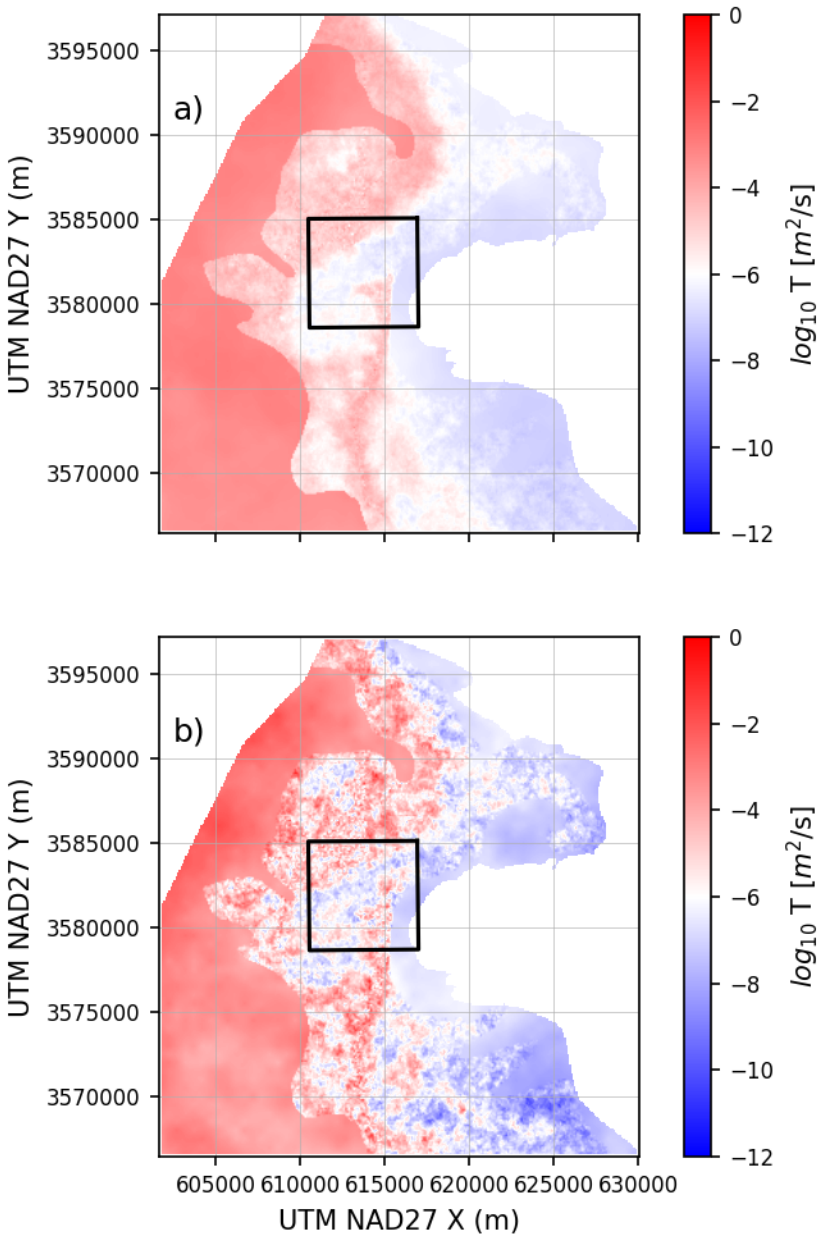


Figure HYDRO-6. Average Transmissivity Across Initial (a) and Calibrated (b) Realizations

HYDRO-3.0 GEOCHEMICAL DATA ACQUISITION AND ANALYSES

Traditional groundwater sampling approaches often rely on purging several wellbore volumes to obtain representative formation water, but this method can be inefficient or poorly suited to low yield or heterogeneous formations such as the Culebra. Beginning in 2017, Culebra water quality samples were collected using a Snap-Sampler down-hole pneumatic sampling tool, which enabled cost-effective and repeatable depth-specific formation sampling in applicable WIPP monitoring wells. These samples were analyzed for pH, specific conductance, and cation/anion balance, as documented in Lofton (2021). Figure HYDRO-7 presents the average cations and anion concentrations across the WIPP monitoring network as a function of geographic location.

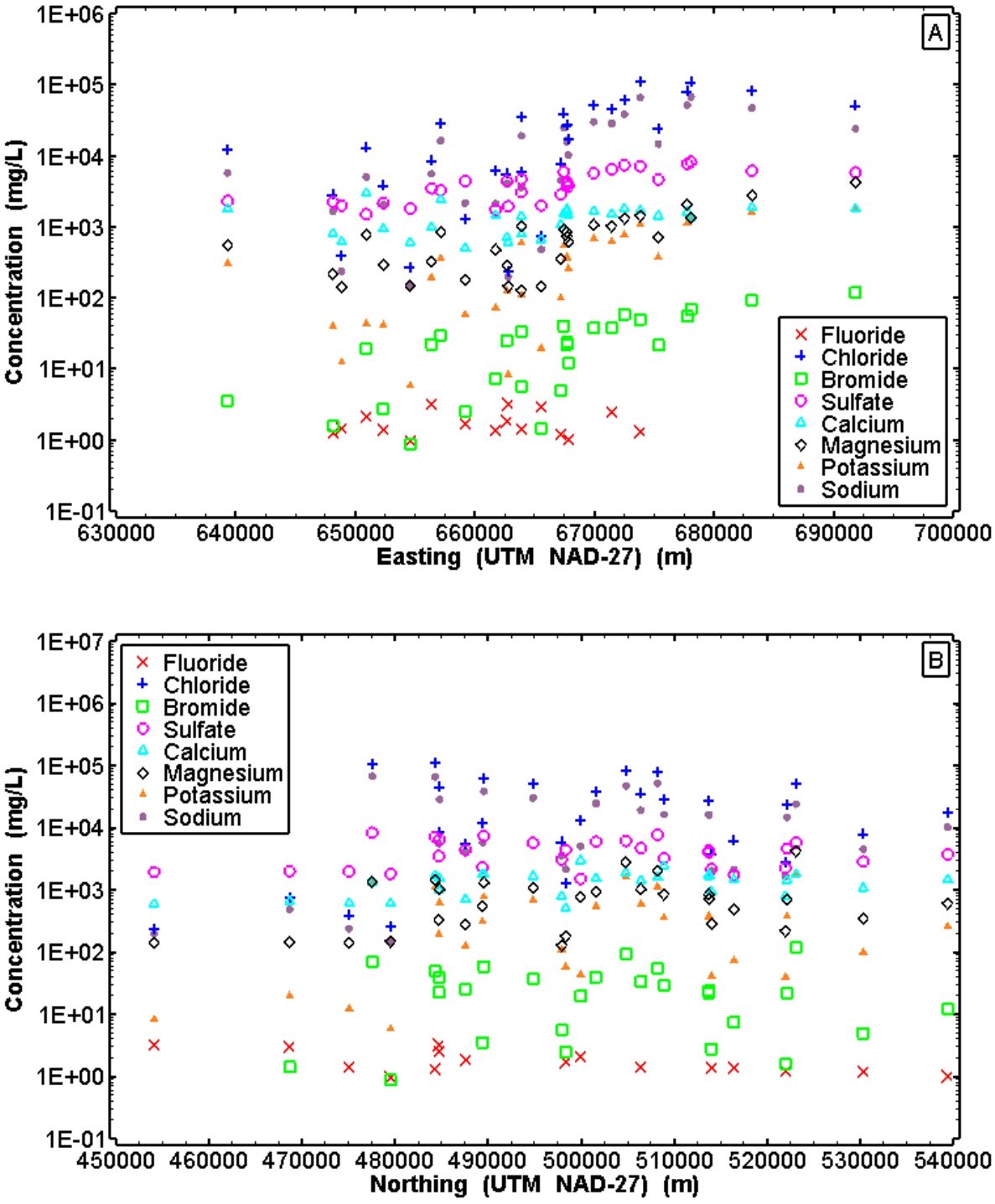


Figure HYDRO-7. The Average Cation/Anion Concentrations for Predominant Analytes Sampled in Culebra WIPP Monitoring Wells with Respect to Longitude (A) and Latitude (B).

Consistent with the requirements of 40 CFR § 194.15(a) to report updates to monitoring data and site characteristics, Kirkes (2022) evaluated Culebra groundwater geochemistry data collected since CRA-2019. The evaluation demonstrates that current groundwater chemistry remains within the historical baseline parameters. This work confirms that the assumptions underlying the Culebra conceptual model approved in previous recertification decisions remain valid.

Kirkes et al. (2022) analyzed existing data to address the identified weakness and create a platform for future work that could further address the concerns from the Culebra conceptual model peer review. Geochemical analyses were conducted on Culebra groundwater samples to gain a better understanding of the predominant hydrogeochemical processes that reflect Culebra hydrology (Kirkes 2022). The study conducted a comparison of geochemistry data to established hydrogeochemical facies (Domski and Beauheim 2008) and flow directions in the Culebra. Conclusions from (Kirkes 2022) were confirmatory of historical hydrogeological baselines. The additional geochemical data and insights further validate the conceptual model approved in previous recertifications. These data confirm that no changes to the Culebra hydrogeology baseline or the performance assessment parameters are warranted under 40 CFR § 194.15(a). Findings and updates from Kirkes et al. (2022), based on geochemical and historical data spanning 1972–2021, include the following:

1. The hydrogeochemical facies of the Culebra, initially defined by Siegel et al. (1991), were updated incorporating results from Domski and Beauheim (2008) and new data since CRA-2019. (Figure HYDRO-8).
2. Sodium-chloride (Na-Cl) and calcium-magnesium-chloride (Ca-Mg-Cl) were corroborated as the dominant major-ion compositions as demonstrated by Piper diagrams and correlation analyses (Figures HYDRO-9 and HYDRO-10).
3. Mineral dissolution and cation-exchange processes were linked to specific regions of the WIPP monitoring network, indicating spatial variability in geochemical controls across the Culebra.
4. The expanded dataset supported Siegel et al.'s (1991) hypothesis that Culebra waters are not in equilibrium with dolomite and that magnesium (Mg^{2+}) enrichment, primarily in facies A and E, is consistent with dissolution of accessory minerals such as carnallite or polyhalite.
5. The geochemical facies data physically validate the spatial boundaries of the high-diffusivity zones used in the approved Culebra flow model.

The hydrogeochemical facies map was updated based on geochemical data from 1978 to 2021, including wells not previously considered (Kirkes et al. 2022). These facies were represented as zones by Siegel et al. (1991) and were further refined by Domski and Beauheim (2008). Key changes include revising the Zone A boundary to reclassify wells WQSP-2 and WIPP-19 into facies Zone A/C, achieved by straightening and extending the Zone A division to better reflect current data. A new facies division for Zone E was added, estimated from wells with similar chemistry (SNL-6, SNL-15, AEC-7R) and the Mudstone/Halite margin locations. These updates

incorporate recent data from several replacement wells installed since 2007, improving the accuracy and spatial representation of facies zones across the study area.

Changes to the boundaries between the major facies are shown in Figures HYDRO-8 and HYDRO-9. Transition facies are not delineated on the map because there is spatial over-lap between the zones and distinct boundaries cannot be definitively determined at this time. A brief description of the key characteristics of each facies is summarized below.

- Facies Zone A:
  Located in the eastern Culebra network, this zone is characterized by relatively low transmissivity and high ionic strength (1.66–5.3 molal). The Mg^{2+}/Ca^{2+} molar ratio (1.07–2.57) indicates dolomite is in saturated to supersaturated states. Water chemistry is dominated by Na-Cl type waters with strong correlations among Mg^{2+}, Na^{+}, K^{+}, Cl^{-}, SO_4^{2-}, and Br^{-}, suggesting the presence of evaporite minerals such as halite, sylvite, polyhalite, and carnallite. Geochemical reactions include gypsum dissolution leading to calcite and dolomite formation, with dolomite dissolution occurring under specific conditions. Cl^{-}/Br^{-} ratios indicate gypsum-containing halite leaching. Some wells show unique chemistry, indicating mineralogical transitions within the zone.
- Facies Zone A/C:
  Situated in the north-central region, this transitional zone has ionic strength between 1.07 and 1.6 molal and Mg^{2+}/Ca^{2+} ratios of 0.85–1.25, consistent with dolomite saturation. Waters are Na-Cl type with ion correlations suggesting minerals like halite, carnallite, and possibly Na-SO_4 minerals. Ca^{2+} is less prominent and negatively correlated with SO_4^{2-}, indicating low anhydrite presence. Cl^{-}/Br^{-} ratios reflect gypsum-containing halite leaching.
- Facies Zone B:
  Located in the southernmost area, this zone exhibits the lowest ionic strength (<0.1 molal) and Mg^{2+}/Ca^{2+} ratios (0.28–0.51), indicating dolomite undersaturation and potential dissolution. Waters are Ca-Mg-Cl type with strong correlations among Ca^{2+}, SO_4^{2-}, Na^{+}, K^{+}, and Cl^{-}, suggesting gypsum dissolution and calcite precipitation. Transmissivity is high, likely enhanced by gypsum dissolution. Cl^{-}/Br^{-} ratios are the lowest in the network, though Br^{-} data are limited.
- Facies Zone B/C:
  A transitional zone scattered mainly along the Salado dissolution line and Nash Draw boundary, with ionic strength of 0.18–0.29 molal and Mg^{2+}/Ca^{2+} ratios of 0.39–0.6. Waters show mixed Na-Cl and Ca-Mg-Cl types. Ion correlations suggest presence of dolomite, calcium chloride, halite, and carnallite, with gypsum largely absent. Cl^{-}/Br^{-} ratios vary widely, indicating complex mixing and possible anthropogenic influences.
- Facies Zone C:
  The largest zone in the network, with ionic strength 0.30–1.02 molal and Mg^{2+}/Ca^{2+} ratios of 0.39–0.99. Waters are predominantly Na-Cl type with strong correlations among Ca^{2+}, Mg^{2+}, Na^{+}, and Cl^{-}, and absence of gypsum. Carbonate species strongly influence pH. Calcite and dolomite are at or above saturation, while magnesite

saturation varies. This zone includes the greatest number of wells and shows complex geochemical interactions.

- Facies Zone D:
  Located in the far western area, this zone includes two abandoned wells (WIPP-27 and WIPP-29) with historical data indicating contamination from potash mining. Due to abandonment and lack of recent data, this zone was not extensively analyzed.
- Facies Zone E:
  In the far eastern portion, this zone includes wells SNL-6, SNL-15, and newly added AEC-7R. Characterized by unique chemistry likely influenced by evaporation and halite dissolution near Mudstone/Halite margins. AEC-7R, although having slightly lower ionic strength, shares chemical characteristics consistent with zone E.

Cation exchange in wells was determined through the integration of geochemical analysis and correlation analyses. Kirkes et al. (2022) implemented the methodology described by Wu et al. (2021), which entails plotting the difference between (Mg^{2+} + Ca^{2+}) and (HCO_3^- + SO_4^{2-}) against the difference between (Na^+ + K^+) and Cl^-. Wells exhibiting slopes ranging from –0.8 to –1.2 on this plot were classified as undergoing cation exchange between Na^+ and Ca^{2+}. Further evaluation of Ca^{2+} versus Ca^{2+} + SO_4^{2-} ratios facilitated differentiation between ion exchange and reverse ion exchange, with numerous wells demonstrating elevated Ca^{2+} consistent with reverse ion exchange (Na^+ adsorbing onto rock and subsequently releasing Ca^{2+} into solution). The pronounced correlation with a slope near –1 (R^2 = 0.9912) provided robust confirmation that cation exchange is a predominant geochemical mechanism in these wells.

Identifying cation exchange processes is crucial because it directly influences groundwater chemistry by altering the concentrations of key ions such as Na^+ and Ca^{2+}. This affects mineral dissolution and precipitation reactions, which control water quality and the mobility of contaminants. Understanding whether ion exchange or reverse ion exchange is occurring provides insight into the sources of dissolved ions and the geochemical evolution of groundwater. Moreover, recognizing cation exchange improves the accuracy of hydrogeochemical models used to predict contaminant transport and assess the long-term safety of subsurface environments like the Culebra formation near WIPP.

The Culebra hydrogeochemical facies were remapped using high-resolution, contemporary monitoring data (Kirkes et al. 2022). The resulting distribution is highly consistent with historical water-type classifications, further reinforcing the robustness and spatial accuracy of the approved conceptual models utilized in previous performance assessments. These localized refinements reduce uncertainty regarding regional groundwater chemistry and spatial variability. The high-resolution data reinforce the conservative assumptions of contaminant transport already established in the WIPP Performance Assessment, confirming the long-term stability of the repository's compliance margin. Confirmation of dominant water types and key geochemical processes such as mineral dissolution and cation exchange informs and enhances groundwater flow and reactive transport models. The finding that equilibrium with dolomite is not maintained and that magnesium is introduced from evaporite minerals underscores the

complexity of water-rock interactions affecting water quality. Additionally, the localized confirmation of gypsum dissolution in the high-diffusivity zone is consistent with the established conceptual models of solute transport in the southern LWB. These findings reinforce the conservative assumptions embedded in the approved performance assessment and support the design of long-term monitoring programs by validating existing flow-pathway predictions. Collectively, these insights augment the extensive body of historical data, reinforcing the high-resolution hydrogeologic characterization and monitoring programs that support the DOE's continued demonstration of compliance under 40 CFR § 194.15(a).

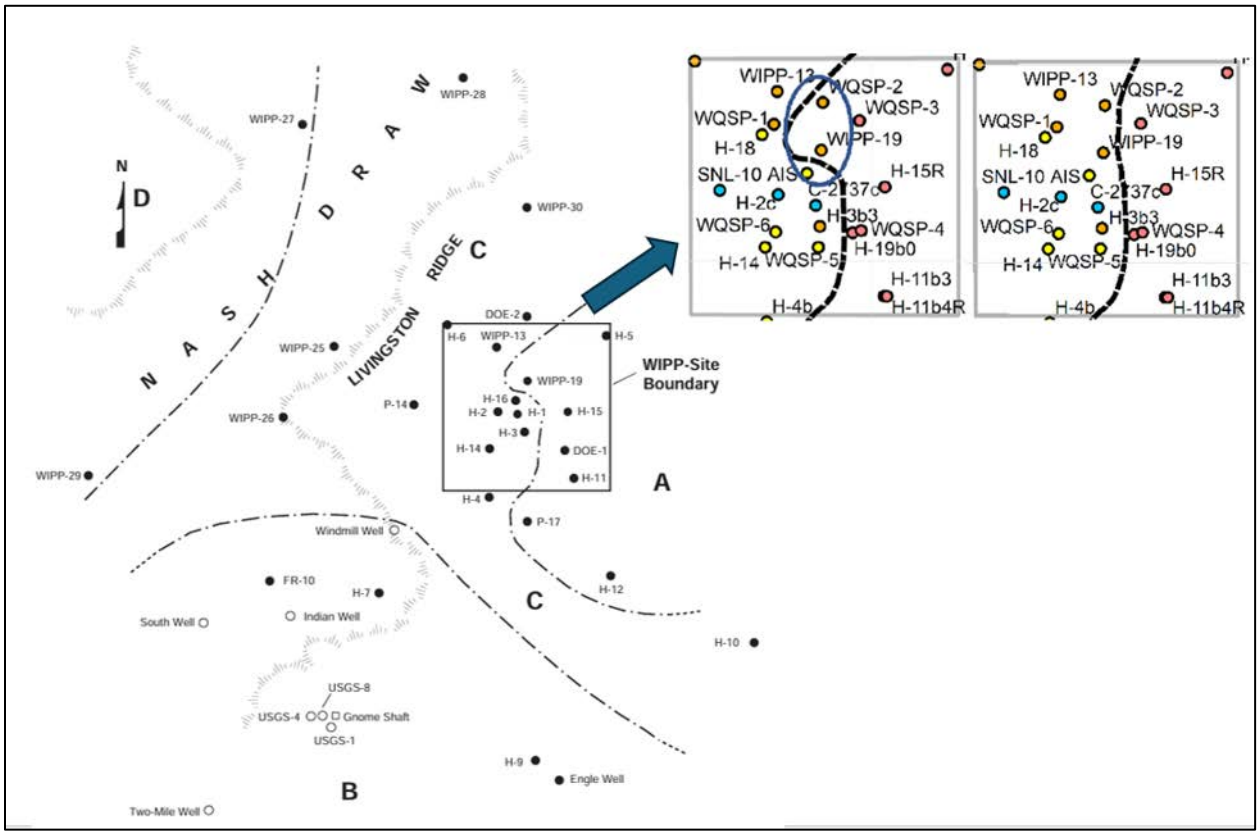


Figure HYDRO-8. Update of Culebra Hydrogeochemical Facies A from Siegel et al. (1991)

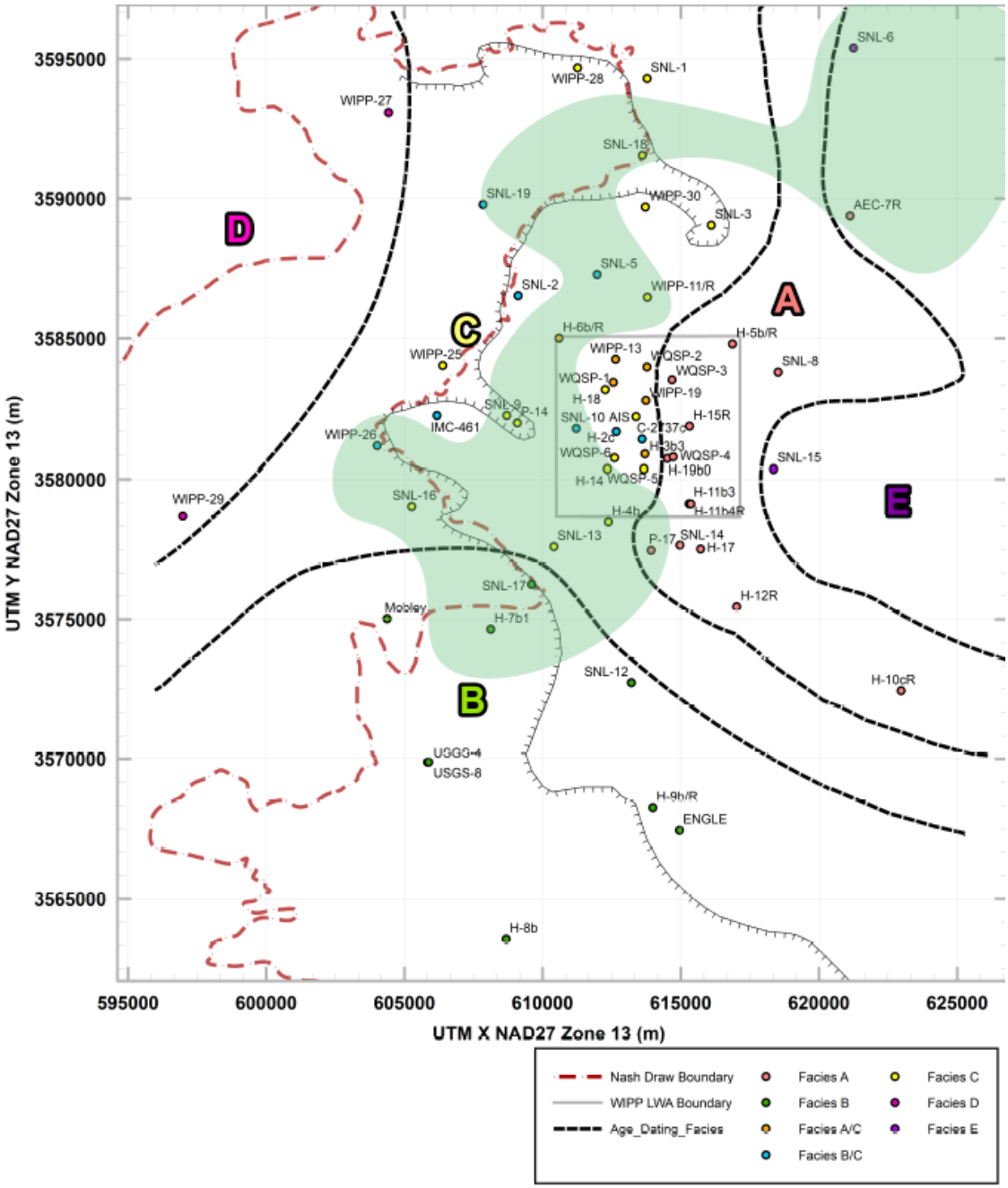


Figure HYDRO-9. Updated Culebra Hydrogeochemical Facies (Kirkes et al. 2022). The Green Area Denotes Cation Exchange Between Na^{+} and Ca^{2+}. Note that the well labeled SNL-17 is well SNL-17a.

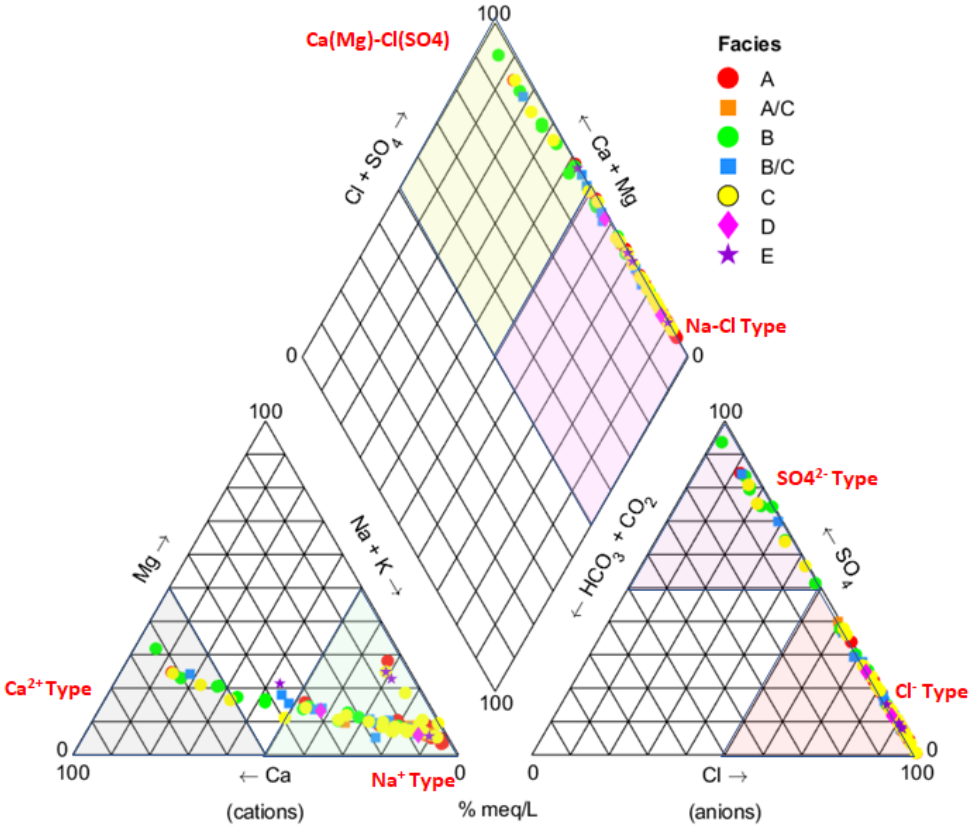


Figure HYDRO-10. Piper Diagram of Samples from the Culebra Well Network (Kirkes et al. 2022)

HYDRO-4.0 GEOLOGICAL INFORMATION

On December 12, 2016, drilling commenced on a pre-shaft corehole (C-3977) at the proposed location of a new utility shaft. Core was collected from a depth of 3.7 m (12 ft) to 703 m (2,308 ft) to obtain reference samples and provide direct information geological conditions (Powers et al., 2018). The hole was logged in the open-hole and in casing with a suite of geophysical tools, including spectral gamma at a 0.8 m (0.25-ft) interval. Core from selected intervals were selected for laboratory testing to quantify geotechnical parameters (Powers et al., 2018).

Stratigraphy and lithologies in C-3977 compared well to those in the air intake shaft, with no evidence of water inflow in the upper 61 m (Berino Soil, Mescalero Caliche, Gatuña, Santa Rosa, and upper Dewey Lake). The Rustler Formation was encountered from a depth of 153.5 m (503.5 ft) to 250.5 m (822 ft). The Magenta Dolomite Member (Magenta) occurred from 563.9 ft - 588.8 ft (171.9 m - 179.5 m) resulting in a thickness of 7.6 m (~25 ft) that is similar to reference Air Intake Shaft (Powers et al., 2018). The Culebra Dolomite Member (Culebra) occurred from 679.7 ft - 701.3 ft (207.2 - 213.8 m) giving a thickness of 6.7 m (~22 ft). The depths and lithology of the four informal hydrostratigraphic units designated CU-1 to CU-4 by

Holt (1997) are consistent with observations in the AIS. Unit CU-1 had little visible porosity with the lower portion containing increased porosity in zones parallel to bedding. Unit CU-2 had a much greater porosity that gradationally increased from Unit CU-1. The lower portion contained large pores and silt-filled pores. Unit CU-3 was very porous, and core return collapsed to rubble. Unit CU-4 was brecciated and deformed over a distorted boundary with the lower Los Medaños Member. The Salado Formation contact at C-3977 occurred at a depth of 250.5 m (822 ft). A stratigraphic column is illustrated in Table HYDRO-1. Additionally, four holes were drilled and cored around the perimeter of C-3977 (C-3976-1 through -4). These holes were drilled to depths ranging from ~40 m (130 ft) to ~61 m (200 ft) to determine if natural shallow groundwater was present above the natural cement change in the upper Dewey Lake Formation (Powers et al. 2019a-d).

Table HYDRO-1. Geology at Borehole C-3977 (Pre-Shaft Core hole) modified from Powers et al. (2018).

Era	Period/ Epoch	Formation or Unit	Member or Marker Bed (MB)	Depth Below Surface by Core Markings	Depth Below Surface by Gamma/Density Log[3]
Cenozoic	Holocene	Surface dune sand and Berino soil	N/A	Drilled to ~3.7 m	N/A
Cenozoic	Pleistocene	Mescalero caliche	N/A	3-3.7 m from cuttings	N/A
Cenozoic	Miocene–Pleistocene	Gatuña	N/A	? - 8.4 m?	~3.7 m - 7.9 m
Mesozoic	Triassic	Santa Rosa	N/A	8.4 m? - 9.8 m?	7.9 m? - 10.4 m
Mesozoic	Triassic	Dewey Lake[1]	N/A	9.8 m – 153.5 m	10.4 m - 153.5 m
Paleozoic	Permian	Rustler (153.5–250.5 m)	Forty-niner	153.5 m – 171.9 m	153.5 m - 171.3 m
Paleozoic	Permian	Rustler (153.5–250.5 m)	*A-5*	153.5 m – 162.6 m	153.5 m - 161.7 m
Paleozoic	Permian	Rustler (153.5–250.5 m)	*M-4/H-4*	162.6 m - 166.3 m	161.7 m - 166.4 m
Paleozoic	Permian	Rustler (153.5–250.5 m)	*A-4*	166.3 m - 171.9 m	166.4 m - 170.8 m
Paleozoic	Permian	Rustler (153.5–250.5 m)	Magenta Dolomite	171.9 m - 179.5 m	170.8 m - 179.1 m
Paleozoic	Permian	Rustler (153.5–250.5 m)	*Tamarisk*	179.5 m - 207.2 m	179.1 m - 206.8 m
Paleozoic	Permian	Rustler (153.5–250.5 m)	*A-3*	179.5 m - 197.3 m	179.1 m - 196.9 m
Paleozoic	Permian	Rustler (153.5–250.5 m)	*M-3/H-3*	197.3 m - 202.7 m	196.9 m - 202.2 m
Paleozoic	Permian	Rustler (153.5–250.5 m)	*A-2*	202.7 m - 207.2 m	202.2 m - 206.8 m
Paleozoic	Permian	Rustler (153.5–250.5 m)	Culebra Dolomite	207.2 m - 213.8 m	206.8 m - 213.2 m
Paleozoic	Permian	Rustler (153.5–250.5 m)	Los Medaños	213.8 m – 250.5 m	213.2 m - 249.6 m
Paleozoic	Permian	Rustler (153.5–250.5 m)	*M-2/H-2*	213.8 m - 216.5 m	213.2 m - 216.3 m
Paleozoic	Permian	Rustler (153.5–250.5 m)	*A-1*	216.5 m - 219.4 m	216.3 m - 219.0 m
Paleozoic	Permian	Rustler (153.5–250.5 m)	*M-1/H-1*	219.4 m - 250.5 m	219.0 m - 249.6 m

Era	Period/ Epoch	Formation or Unit	Member or Marker Bed (MB)	Depth Below Surface by Core Markings	Depth Below Surface by Gamma/Density Log[3]
Paleozoic	Permian	Salado (250.5 m–TD)	MB103	301.8 m - 306.4 m	301.4 m - 306.0 m
Paleozoic	Permian	Salado (250.5 m–TD)	MB109	340.2 m - 348.4 m	339.9 m - 347.8 m
Paleozoic	Permian	Salado (250.5 m–TD)	Vaca Triste	401.4 m - 403.6 m	400.8 m - 403.6 m
Paleozoic	Permian	Salado (250.5 m–TD)	Union Anhydrite	458.4 m - 460.5 m	457.5 m - 459.3 m
Paleozoic	Permian	Salado (250.5 m–TD)	MB123–124	483.0 m - 489.5 m	481.9 m - 488.6 m
Paleozoic	Permian	Salado (250.5 m–TD)	MB134	590.1 m - 593.5 m	589.2 m - 592.5 m
Paleozoic	Permian	Salado (250.5 m–TD)	MB136	611.7 m - 614.6 m	610.5 m - 613.6 m
Paleozoic	Permian	Salado (250.5 m–TD)	MB139	649.3 m - 650.6 m	648.3 m - 649.5 m
Paleozoic	Permian	Salado (250.5 m–TD)	MB140	666.6 m - 670.4 m	665.4 m - 669.3 m
Paleozoic	Permian	Salado (250.5 m–TD)	MB142	702.8 m – TD[2]	Not logged – tool to 687.6 m

[1]The bottom of the Dewey Lake formed in the Permian
[2]TD marked on core 2,311.1 ft (704.4 m)
[3]Subtracted 3 ft (0.9 m) for surf. elev.

HYDRO-5.0 WELL REPLACEMENT

Monitoring wells completed with steel casing are routinely plugged and abandoned or replaced because of corrosion. Since the CRA-2019, 10 steel-cased monitoring wells completed in the Culebra have been plugged and abandoned (Table HYDRO-2). Between 2018 and 2025, the only new monitoring wells that were drilled were replacement wells on the WIPP-11 and H-5 well pads These steel-cased wells were replaced/completed with fiberglass-reinforced plastic casings. A well network optimization by Kuhlman (2010) identified nine Culebra wells for plugging and abandonment, indicating that their removal would have minimal statistical impact on Culebra flow-model coverage. H-5c, the only Magenta well, was plugged and abandoned due to a deteriorating casing.

Table HYDRO-2. Wells Plugged and Abandoned 2018—2022

Well	Interval Previously Monitored	Activity	Date of Activity	Current Interval Monitored
WIPP-11	**Culebra**	**Plugged, Well Replaced (WIPP-11R)**	**September 2019**	**WIPP-11R Culebra**
H-5b	**Culebra**	**Plugged, Well Replaced (H-5bR)**	**September 2019**	**H-5bR Culebra**
H-5c	**Magenta**	**Plugged and Abandoned**	**September 2019**	**N/A**
H-17	**Culebra**	**Plugged and Abandoned**	**April 2020**	**N/A**
WIPP-19	**Culebra**	**Plugged and Abandoned**	**April 2020**	**N/A**

Well	Interval Previously Monitored	Activity	Date of Activity	Current Interval Monitored
H-2b2	Culebra	Plugged and Abandoned	April 2020	N/A
H-3b2	Culebra	Plugged and Abandoned	April 2020	N/A
H-7b1	Culebra	Plugged and Abandoned	April 2020	N/A
WIPP-13	Culebra	Plugged and Abandoned	April 2021	N/A
ERDA-9	Culebra	Plugged and Abandoned	September 2022	N/A

HYDRO-6.0 MONITORING

The monitoring program supports regulatory compliance by tracking groundwater levels and quality across the well monitoring network (U.S. DOE 2023b). The locations of monitored wells are shown in Figure HYDRO-1. Plugged, abandoned, replaced wells are listed in Table HYDRO-2.

The monitoring program includes continuous fluid-pressure measurements at 15 minute (min) intervals using downhole pressure/temperature transducers along with twice-monthly water-level measurements- one per month by each of two monitoring groups- in most network wells. Pressure transducers are installed mid-formation where the full formation thickness is screened. Water levels are used to develop potentiometric surface maps, from which Culebra groundwater flow direction and the travel times of hypothetical contaminant releases to the LWA boundary are calculated. The potentiometric surface maps have been reported in the Annual Site Environmental Reports (ASERs) (U.S. DOE 2019, U.S. DOE 2020, U.S. DOE 2021b, U.S. DOE 2022, U.S. DOE 2023a, U.S. DOE 2024, and U.S. DOE 2025). Water levels are currently being monitored in the Culebra, Magenta, Dewey Lake, and the Bell Canyon Formation.

Pressure-transducer data align with the less frequent manual water-level measurements and clearly record barometric and Earth-tide fluctuations. Typically, barometric and Earth-tide fluctuations are removed from pressure-transducer data prior to analysis using a least-squares barometric response-function approach (Toll and Rasmussen 2007).

HYDRO-6.1 Culebra Monitoring

High-frequency pressure transducer measurements provide a much higher resolution record of hydraulic-head changes than the twice-monthly manual measurements. The high-frequency pressure transducer data shows detailed fluctuations due to both natural (barometric pressure, Earth-tides, and precipitation) and anthropogenic (livestock/production pumping and oil well drilling) effects (Figure HYDRO-11).

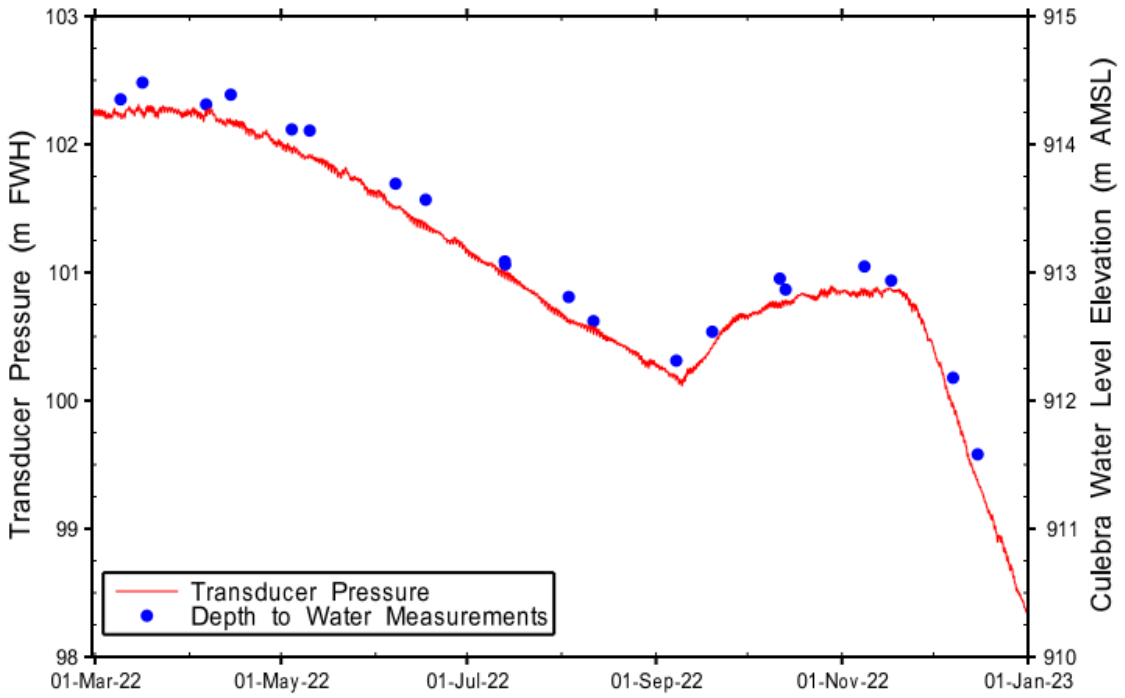


Figure HYDRO-11. Depth to Water Measurements and Pressure Transducer Data for Well C-2737.

Currently, 36 Culebra wells are monitored with downhole pressure transducers, and 34 of these are connected to remote telemetry; wells H-16 and H-19b0 still require systems (see Figure HYDRO-1 for well locations). Figure HYDRO-12 displays the well groupings expressed in hydrographs described in this Appendix HYDRO-6.1. These groupings include:

- Two sets of anthropogenically affected by well C-02348 (Anthropogenic #1, #2),
- Wells that experienced water level decreases due to shaft leakage (Leakage),
- Wells that are in or in close proximity to Nash Draw (Nash Draw),
- Two sets of northern WIPP monitoring wells separated for visual data clarity (North #1, #2),
- Wells with long-term recovery (Increasing), and
- Wells with short-term water level profiles due to plugging and abandonment (Short Term).

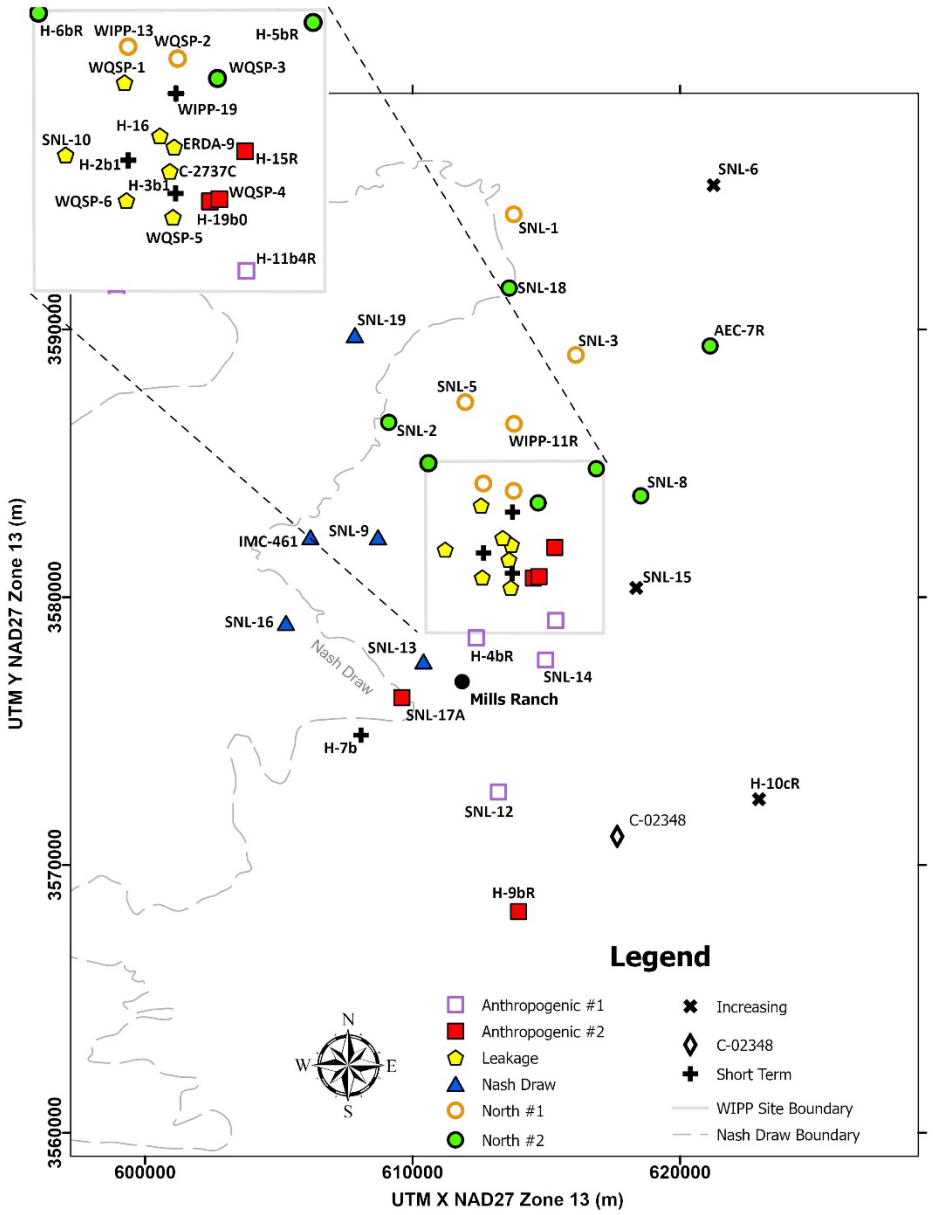


Figure HYDRO-12. Culebra Well Locations and Their Hydrograph Groupings

Culebra groundwater total dissolved solids (TDS) varies from ~3,500 ppm in the southeastern arm of Nash Draw to ~212,000 ppm in deeper, eastern monitoring wells. The range of TDS/densities requires accounting when creating equivalent freshwater head representations across the well network. Groundwater density calculations are performed under Activity/Project-Specific Procedure (SP) 9-11, 'Calculation of Densities for Groundwater in WIPP Wells' (Reyna 2025) to create freshwater head calculations. Pressure transducers are installed at mid-formation, allowing the observed pressure, installation depth, and measured water levels to be combined to estimate fluid density. This procedure is routinely used to calculate fluid densities. Since CRA-2019, fluid density data have been reported by (Johnson 2018, Johnson 2019, Farinacci and Johnson 2020, Farinacci and Johnson 2021, Farinacci and Johnson 2022, Reyna

and Johnson 2023, and Reyna and Johnson 2024). This approach was also used for 2023 Culebra groundwater densities to estimate freshwater heads required for the calibration of the Culebra groundwater flow model for Appendix TFIELD.

The higher-frequency pressure transducer data show that wells near Nash Draw respond rapidly to large rainfall events, whereas wells farther east exhibit muted and delayed pressure pulses transmitted through the higher-diffusivity fracture zone (Hillesheim et al. 2007, Beauheim 2007). These responses support the interpretation that the Culebra is unconfined in parts of Nash Draw and can communicate with overlying stratigraphic units through leakage rather than direct rainfall response. These observations help inform areas of Culebra confinement (confined, unconfined, and transition) in the Culebra flow model used in generating T-fields (see Appendix TFIELD). The eastern-most responses are likely caused by a rainfall-generated pressure wave propagating horizontally through the Culebra, rather than by vertical recharge at the observation point.

Figure HYDRO-14 through Figure HYDRO-22 show manual water level elevation in Culebra wells monitored between 2018 and 2025. Wells are grouped together roughly by geographic locality and commonly affected water levels.

HYDRO-6.2 Normalized Hydrograph

Bowman (2025) created a hydrograph of the full set of measured water levels for wells in the WIPP monitoring network. The water level measurements were screened for anthropogenic effects and normalized utilizing a regression of average heads. This approach was similar in method to the generation of CRA-2026 calibration target heads (Farinacci and Bowman 2022). The resulting water levels were normalized to a zero head value to align WIPP monitoring well network measurements to investigate relative change. A hydrograph of these values is shown in Figure HYDRO-13. Though the head values for individual wells are largely indistinguishable in the hydrograph, the intent is to provide a sense of the general trend of non-anthropogenic Culebra water level measurements over the duration of the monitoring program.

As discussed in the Culebra flow model Peer Review (Burgess et al. 2008), water levels generally increase until 2008. It was hypothesized that this increase was the Culebra recovering from shaft leakage during the initial excavation of the repository. After 2008, water levels the monitored Culebra generally begin to decline steadily. In 2013, water production from the Mills Ranch well (1) created large decreases in water level for many of the monitoring wells close to the southern LWB. Recovery from production began in early 2018 (2), which persisted until 2019. In 2022, salt handling shaft and Shaft #5 leakage (3) began decreasing head in wells inside the LWB. Wells that were unaffected by Mills Ranch production and shaft leakage continued to steadily decline through 2024.

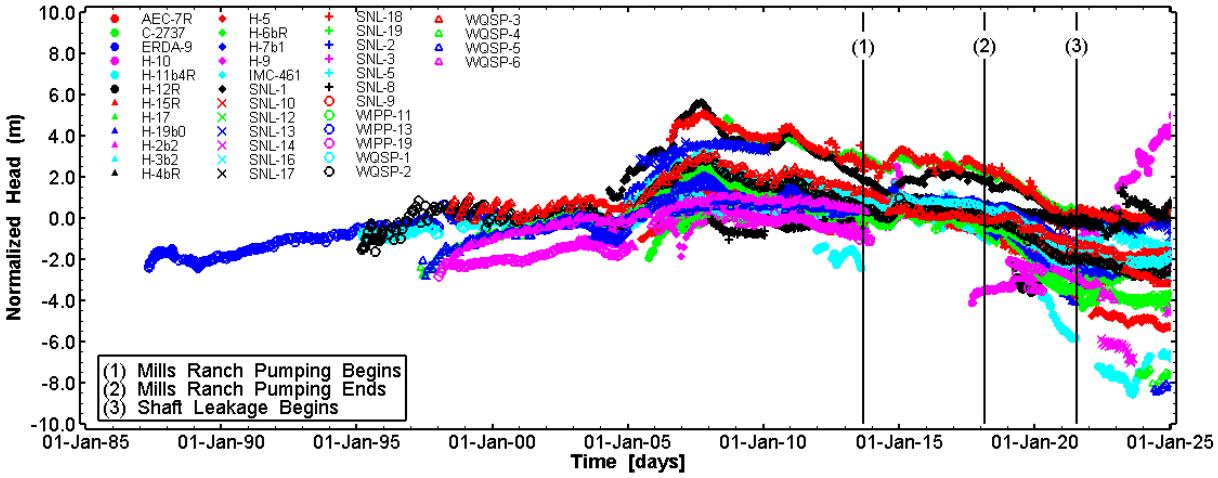


Figure HYDRO-13. A Hydrograph of Normalized Head for All Current WIPP Monitoring Network Wells Screened for Anthropogenic Effects (modified from Bowman 2025).

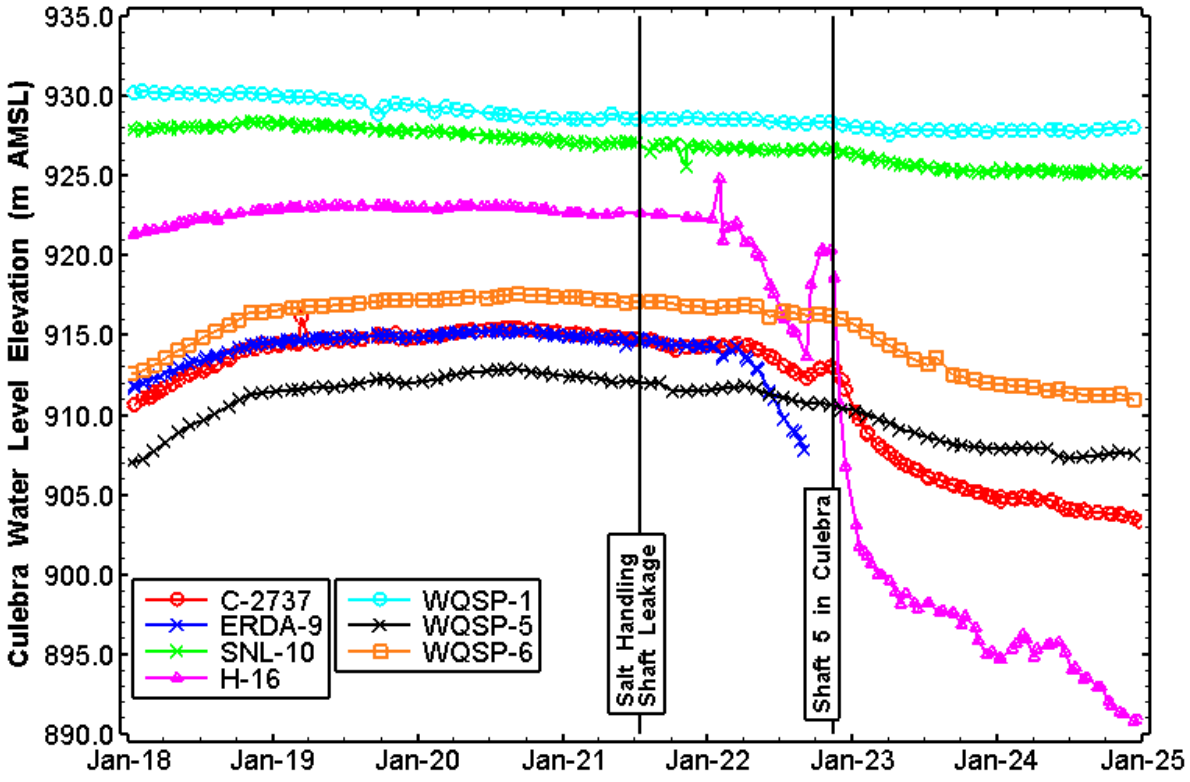


Figure HYDRO-14. Water Level Elevations for Culebra Wells Impacted by Shaft Leakage

The water level elevations plotted in Figure HYDRO-14 show wells that have been affected by leakage in the Salt-Handling Shaft (C-2737, ERDA-9, H-16) and Shaft 5. Water level elevation declines due to leaking in the Salt Handling Shaft began between July and August of 2021. These were later overtaken by leakage into the newly excavated Shaft 5, which first penetrated the Culebra on 11/15/22 (Figure HYDRO-14). The magnitude of the decrease in water level elevation appears to be related to the proximity of the wells to the two shafts. Water level measurements in ERDA-9 stopped in the third quarter of 2022 because the well was removed from the monitoring network. Prior to the leakage, the Culebra water levels in this area were still experiencing recovery from Mills Ranch pumping activities in the years prior (2018) with exception to WQSP-1.

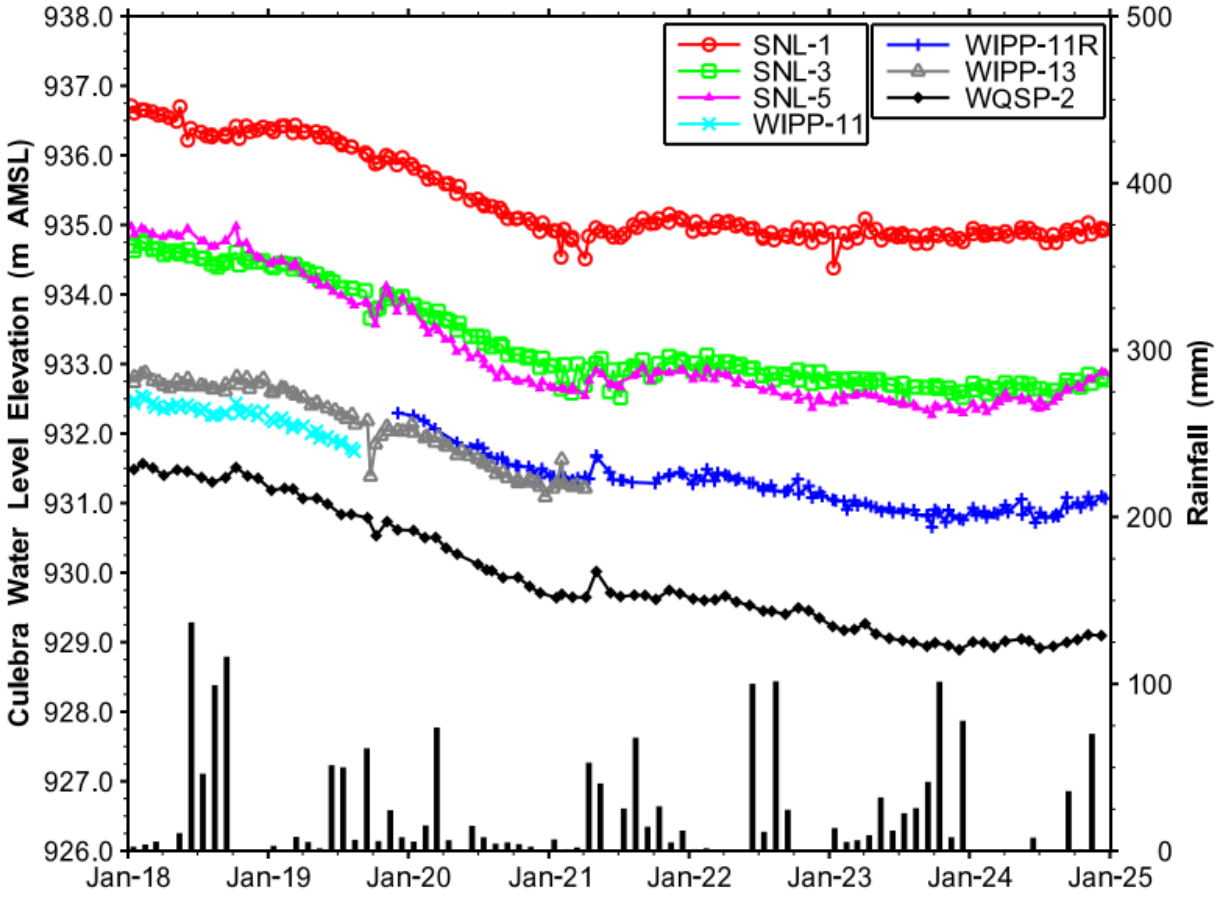


Figure HYDRO-15. Water Level Elevations for Northern Culebra Wells #1

Figure HYDRO-15 shows water level elevations in wells north of and central to the WIPP repository footprint, along with monthly precipitation data from the National Climate Data Center Meteorological Station “WASTE ISOLT N PILOT PLANT” (NOAA 2025). Well WIPP-11 was replaced by WIPP-11R on the same well pad. Wells to the north of the site experienced a uniform decrease in water level elevation between 2018 and 2020, that later stabilized between 2020 and the present. Well WIPP-13 followed similar water level changes but was

plugged and abandoned in 2021. Short-term variations in water levels are observed in northern Culebra wells, some of the water level increases occur during or after precipitation events. Given that these wells are located in confined portions of the Culebra, it is likely that the responses are a product of pressure signal.

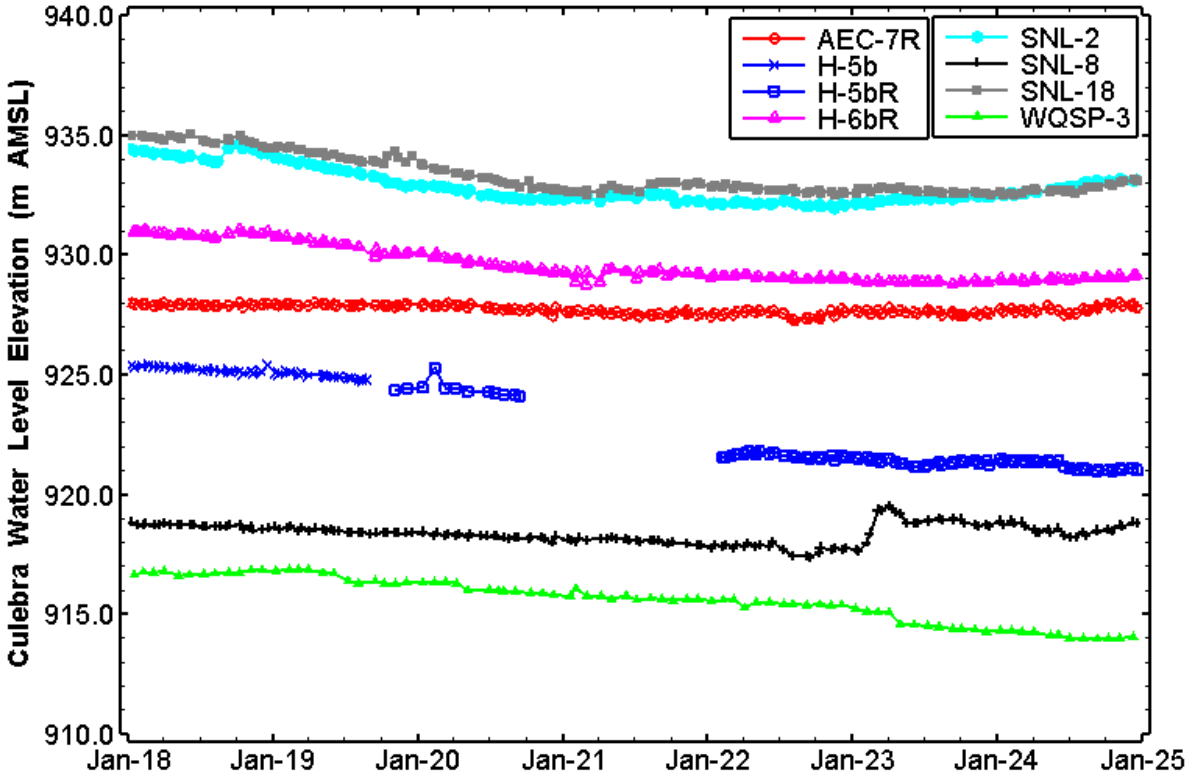


Figure HYDRO-16. Water Level Elevations for Northern Culebra Wells #2

Figure HYDRO-16 shows water levels from eight wells in the northern portion of the Culebra monitoring network. These wells showed small changes in water level from 2018 to the present and, during this time, were largely unaffected by Mills Ranch pumping recovery. Well H-5b was replaced by well H-5bR on the same well pad as well H-5b was an open hole that was prone to repeated collapse. The discontinuity in the H-5bR water levels was due to a pause in data collection while the well was being developed and the water level decrease occurs after the development. Two close oil drilling operations were observed during the step increase in SNL-8 in 2023.

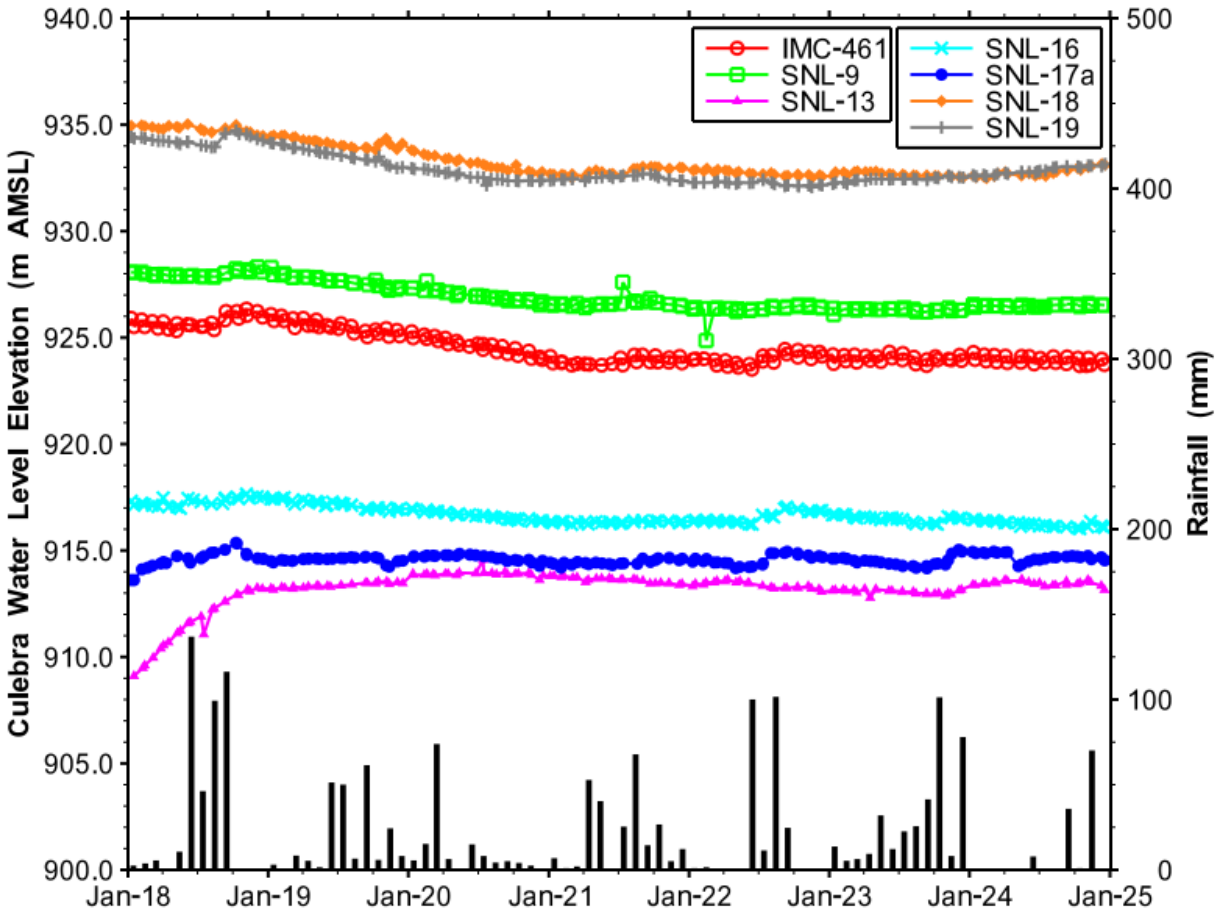


Figure HYDRO-17. Water Level Elevations and Rainfall Data for Culebra Wells Near Nash Draw with Rainfall Data.

Figure HYDRO-17 shows water level measurements for wells in, or near to the southern portion of Nash Draw and includes monthly precipitation data from the National Climate Data Center Meteorological Station "WASTE ISOLT N PILOT PLANT" (NOAA 2025). Wells in proximity to Nash Draw had short-term responses during larger precipitation events but had slightly decreasing water levels from 2018 to the present. Wells SNL-13 and SNL-17a show 2018-2019 recovery from Mills Ranch pumping.

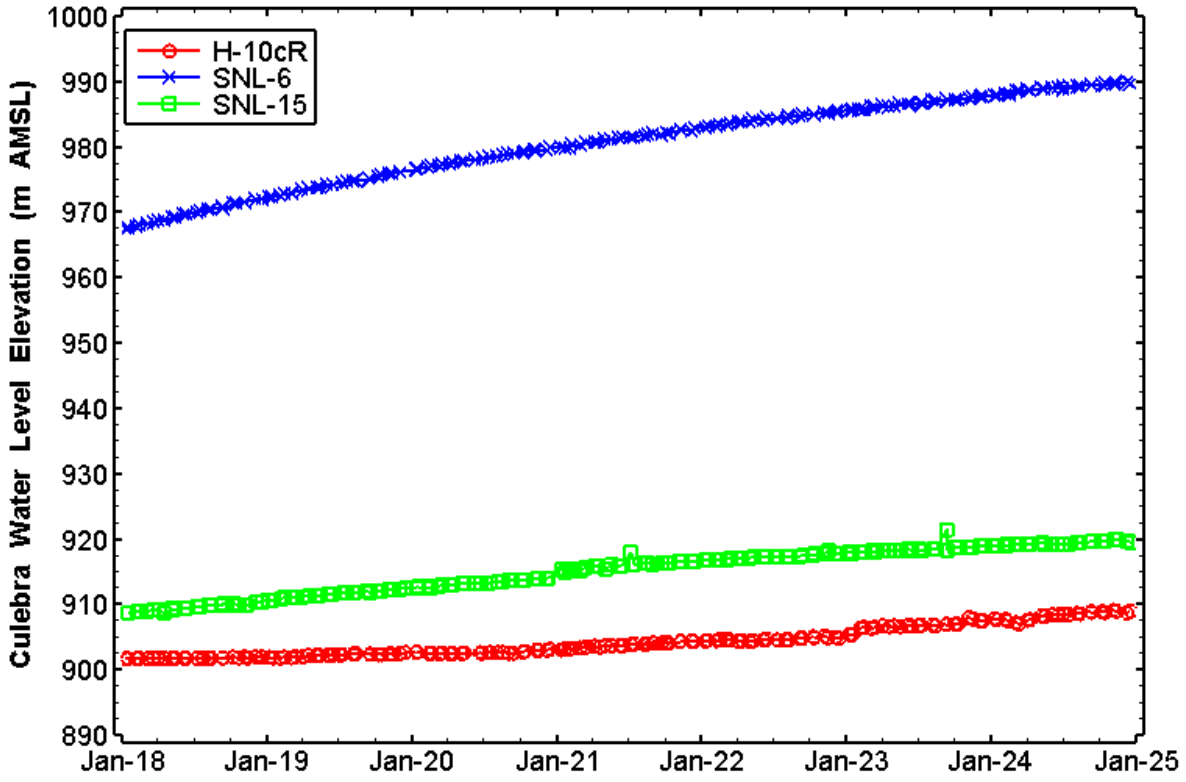


Figure HYDRO-18. Water Level Elevations for Culebra Long-Term Recovery Wells

Figure HYDRO-18 shows water level elevation in Culebra wells H-10cR, SNL-6, and SNL-15. These wells were drilled in the deepest portions of the monitored Culebra to the east, in areas where the Culebra contains halite cement, and their well test analyses produced relatively low transmissivities (H-10cR – 7.41E-08 m^2/s, Bowman 2017; SNL-6 – 8.72E-12 m^2/s, Bowman and Roberts 2009; SNL-15 – 1.38E-13 m^2/s, Roberts 2007). Each well has been slowly recovering since their initial well-development and testing activities. As these wells have been recovering since 2005, 2006, and 2017 (SNL-15, SNL-6, and H-10cR, respectively), their water levels are not representative of undisturbed Culebra conditions. Wells SNL-6 and SNL-15 are east of the M2/H2 halite margin whereas H-10c is to the west of this boundary.

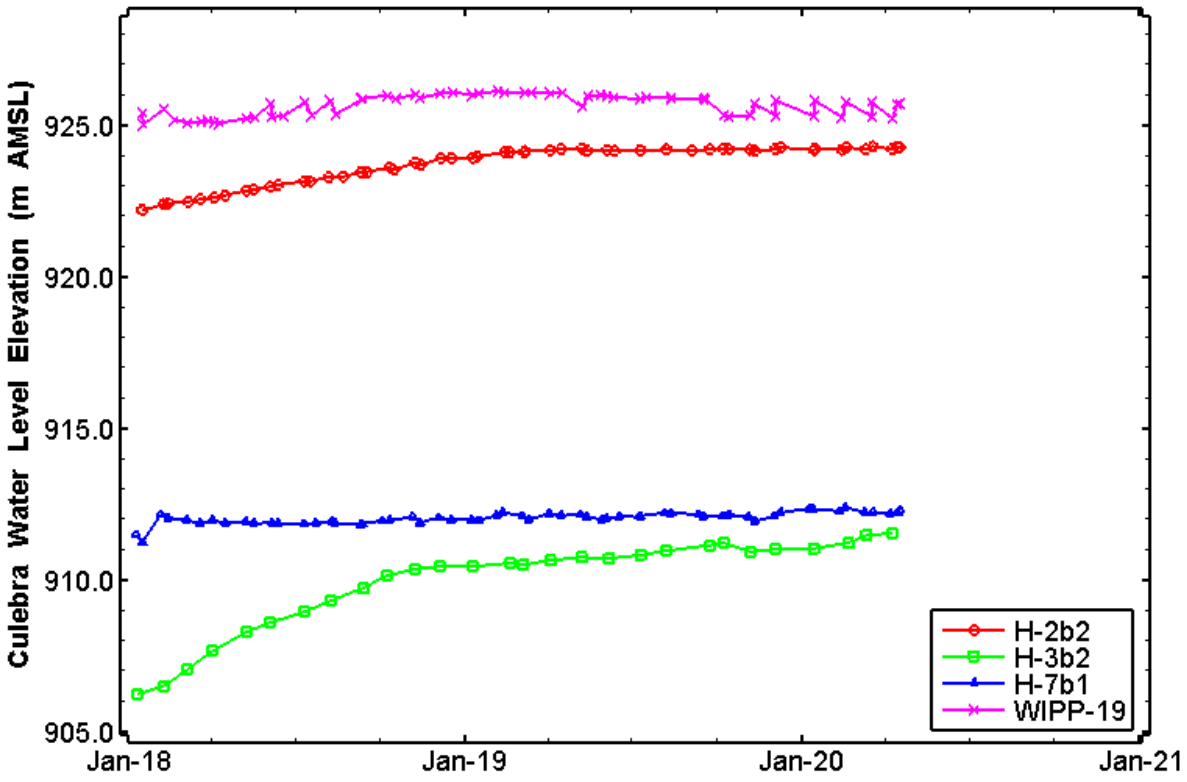


Figure HYDRO-19. Water Level Elevations for Culebra Plugged and Abandoned Wells

Figure HYDRO-19 shows the final water level elevations since CRA-2019 for wells H-2b2, H-3b2, H-7b1, and WIPP-19. The four wells had recovered or were in the final stage of recovery from Mills Ranch pumping when they were plugged (Salness 2006, U.S. DOE 2021a).

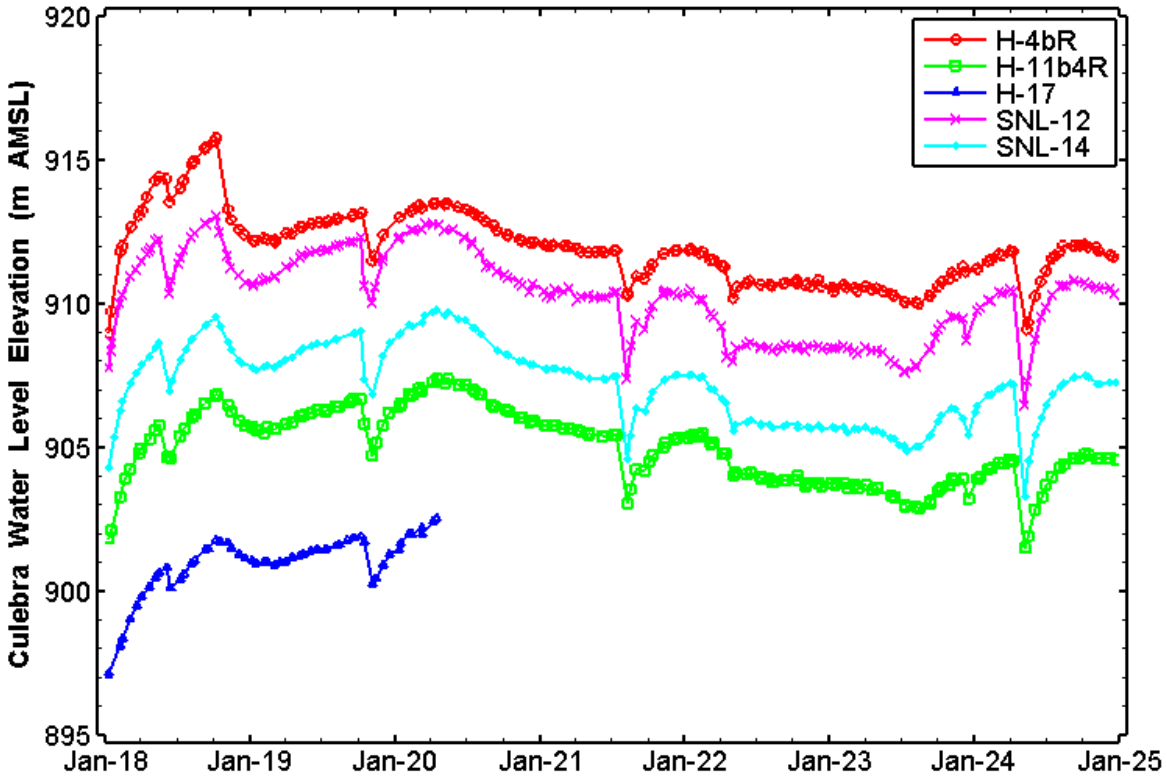


Figure HYDRO-20. Wells with Anthropogenically Affected Water Level Elevations in Close Proximity to Well C-02348.

Figure HYDRO-19 shows water level elevations for wells in the vicinity of livestock well C-02348 to the south of the LWB. Several of these wells exhibit recurring short-term drawdowns followed by gradual recovery, a pattern that is consistent with nearby pumping influences. Well C-02348 (Figure HYDRO-12) is permitted to pump 3 acre-foot of groundwater per year. Although the specific pumping schedule for C-02348 is not available, the similarity and timing of responses among H-4bR, H-11b4R, H-17, SNL-12, and SNL-14 suggest a common localized source of stress. In each case, water levels typically rebound within a few months after each drawdown event. Though these wells are affected by the local pumping, they generally fully recover after a few months. The figure also includes the final set of water level elevations collected from well H-17 after CRA-2019 up until it was plugged and abandoned.

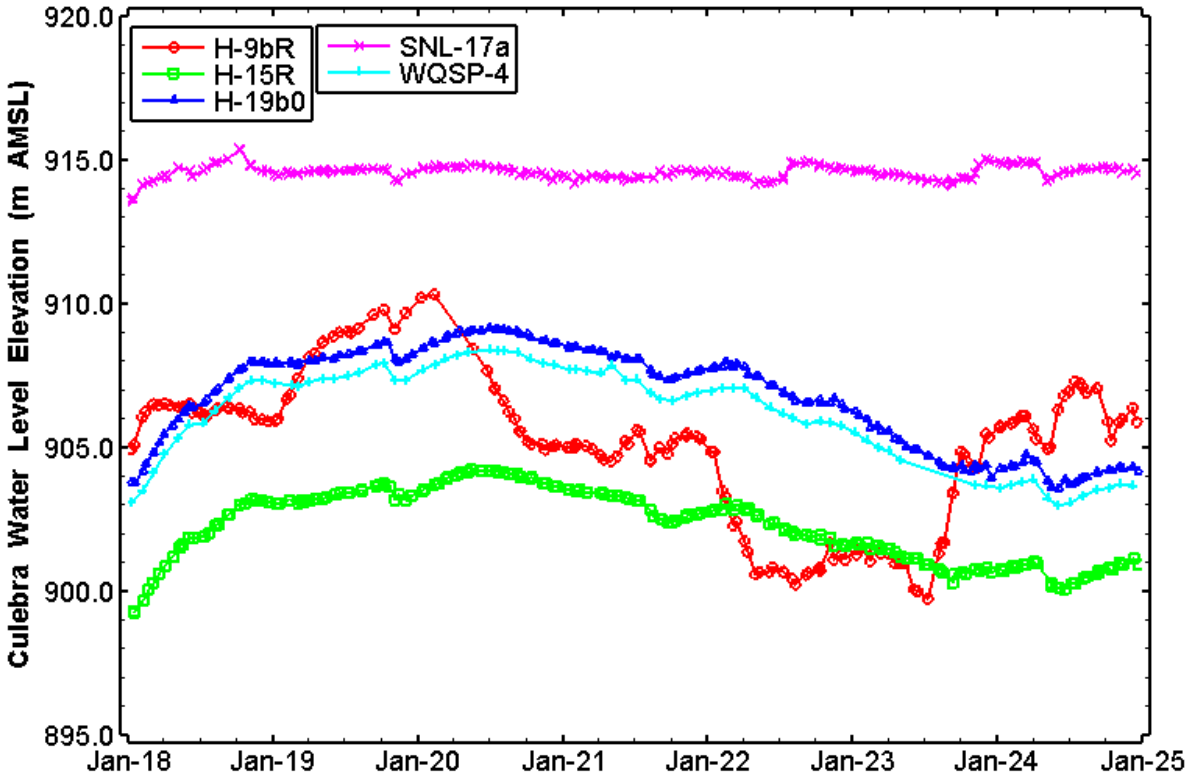


Figure HYDRO-21. Wells with Anthropogenically Affected Water Level Elevations

Figure HYDRO-21 shows water level elevations for wells that exhibit anthropogenic drawdown patterns, although with smaller magnitudes than those observed in wells closest to livestock well C-02348. Early increases in water level are consistent with regional recovery from Mills Ranch pumping. Well H-9bR shows occasional short-term declines followed by recovery, which may be influenced partly by pumping at C-02348. However, H-9bR also displays additional anthropogenic fluctuations unrelated to that well. Well H-9bR is located within an active oil-field drilling zone, and repeated drilling activities, particularly rapid drilling through the Rustler, likely contribute to several of the observed water level changes. Wells H-15R and H-19b0 show more muted variability overall, with gradual long-term trends and limited short-term disturbances.

HYDRO-6.2 Magenta Monitoring

Water levels were monitored in 13 wells completed in the Magenta (9 inside, 4 outside the LWB) (Figure HYDRO-1) during the period of January 2018 through January 2025. The Magenta wells are also instrumented with downhole pressure transducers, programmed to measure pressure head at 15 min intervals. Figure HYDRO-22 shows water table elevations for wells

inside the LWB, whereas Figure HYDRO-23 shows water table elevations for wells outside the LWB.

Figure HYDRO-22 shows water level elevation from eight Magenta wells inside the LWB and includes well H-4c, which was included due to its close proximity to the southern boundary. From 2018 through mid-2019, these wells exhibit generally stable water levels, except for H-15, with small increases of less than one meter. Beginning in mid-2019, all wells show a gradual decline, typically between one and three meters, continuing through mid-2021. Between July and August of 2021, water level elevations begin to decline at an increased rate, and this accelerated decrease persists into 2022 and 2023. The timing and spatial consistency of these water level declines correspond with decreases observed in the Culebra and attributed to seepage into the newly mined Shaft 5.

The response observed in many Magenta wells to the sinking of Shaft 5 represents the farthest propagation of a pressure signal ever documented in the Magenta inside the WIPP monitoring network. No multi-well pumping tests have been conducted in the Magenta, and historically the Magenta has shown very limited cross-well responses during activities in nearby wells. This limited connectivity is largely due to the low permeability of the Magenta, which cannot sustain pumping at rates high enough to generate substantial drawdown. In contrast, the shaft sinking activities produced a significantly larger perturbation than previously recorded in the Magenta, allowing the pressure changes to propagate across a wider portion of the LWB than any earlier event.

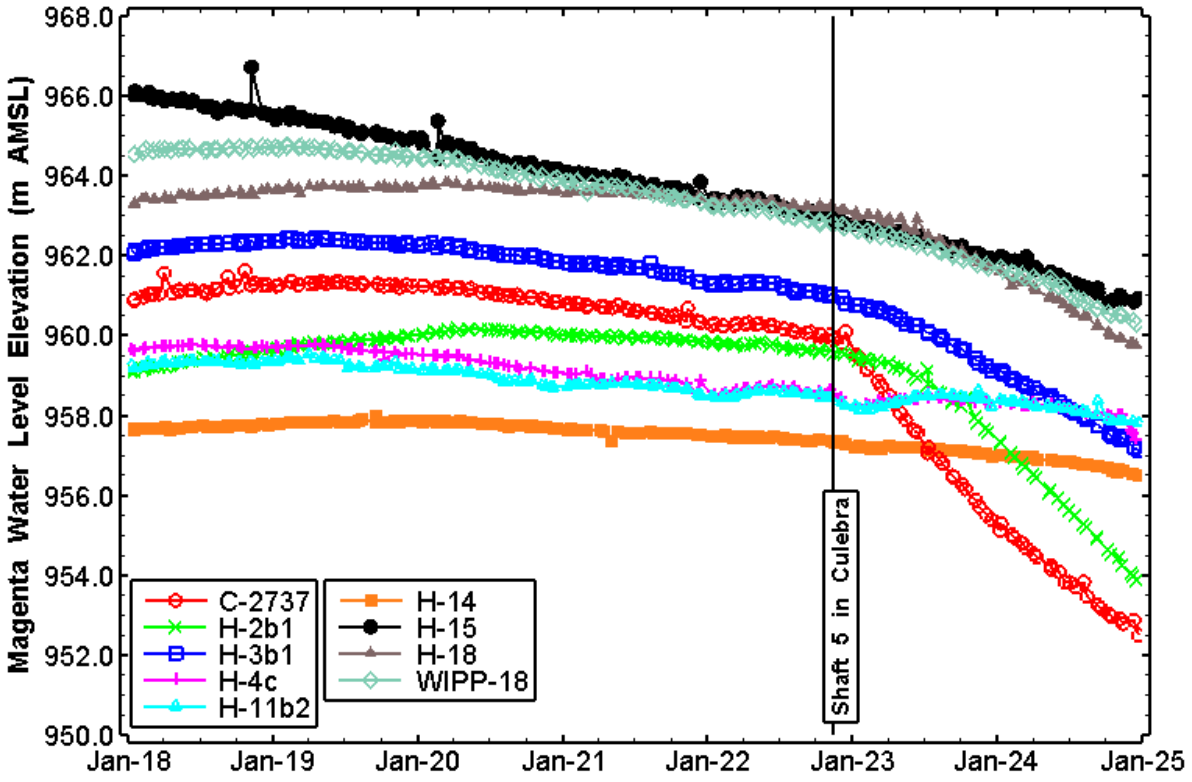


Figure HYDRO-22. Water Level Elevation in Magenta Wells Inside the LWB

Figure HYDRO-23 shows water level elevations from four Magenta wells on or outside the LWB. Although H-4c is just outside the southern boundary, it was addressed with wells inside the boundary (Figure HYDRO-22). From 2018 through early 2022, wells H-9c, H-10a, and H-8a exhibit gradual water level increases, with total rises of up to ~4 m. In contrast, well H-6c, which remains relatively stable through 2021 and then begins to small but persistent decline starting in early 2022. This decrease corresponds temporally to the regional drawdowns observed inside the LWB and attributed to Culebra seepage in Shaft 5 and leakage in the Salt Handling Shaft. However, the magnitude is notably smaller than the responses documented in interior wells.

Prior to November 2022, Magenta water levels inside the LWB showed a gradual decline of up to ~3 m, whereas wells outside the LWB exhibited gradual increases of up ~4 m. In November 2022, simultaneous decreases in both Culebra and Magenta water levels were identified and subsequently attributed to seepage associated with the construction of the new utility shaft.

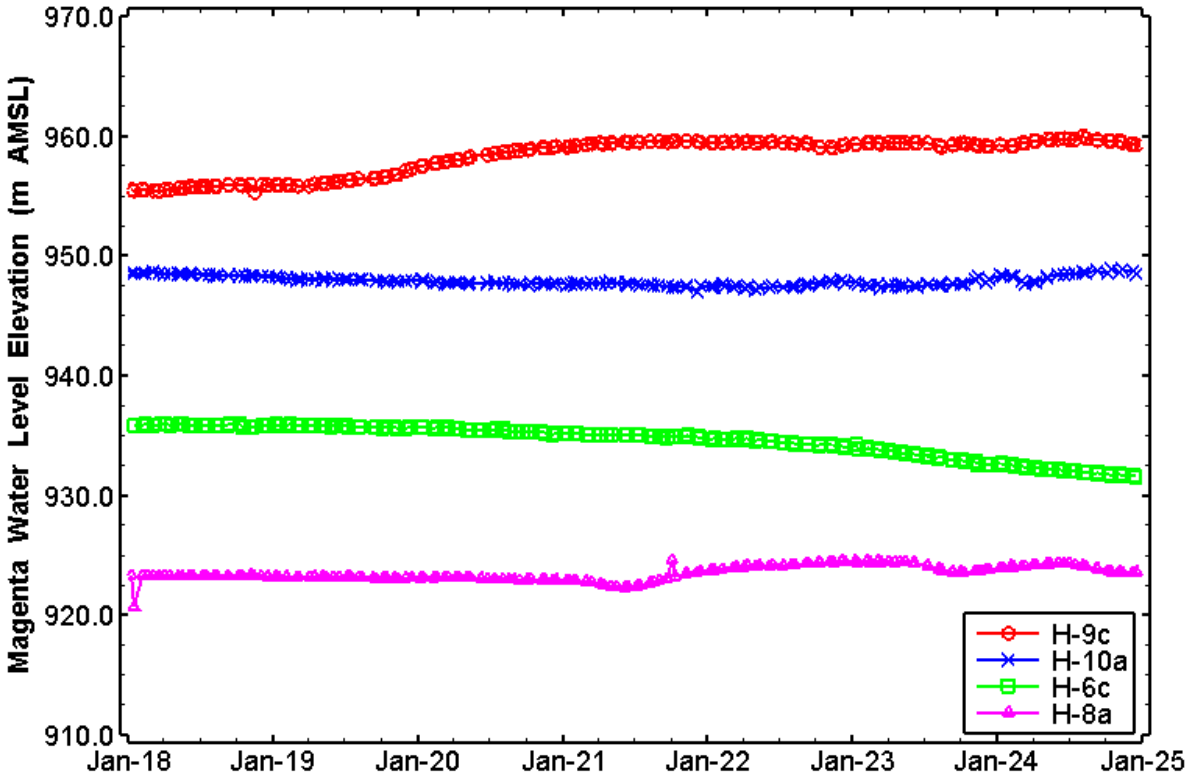


Figure HYDRO-23. Water Level Elevation in Magenta Wells Outside the LWB

HYDRO-6.3 Dewey Lake Monitoring

Water level elevations are monitored in the Dewey Lake in wells PZ-17b and WQSP-6A. HYDRO-24 shows a time series of Dewey Lake water level elevation in WQSP-6A from January 2018 through January 2025. The hydrograph shows water levels with a slight downward trend. Well PZ-17b was installed as a monitoring well down-gradient from facultative lagoons for contamination detection to the Dewey Lake.

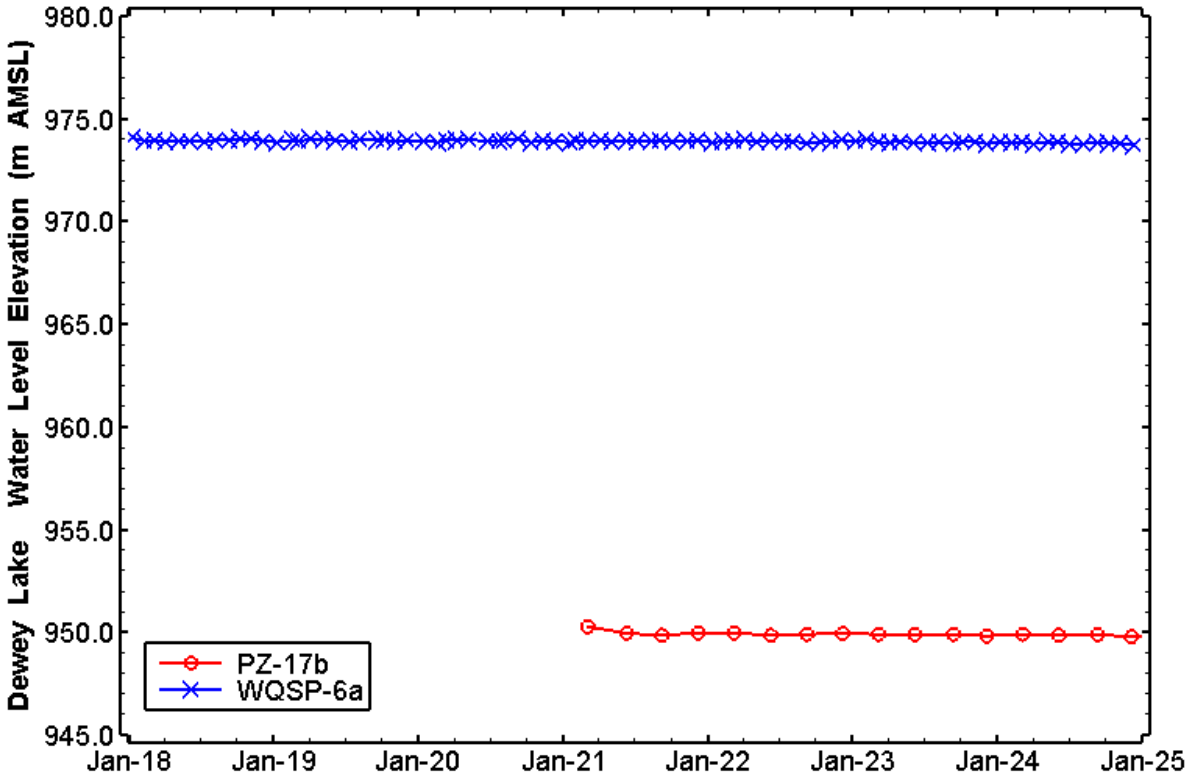


Figure HYDRO-24. Dewey Lake Water Levels

HYDRO-6.4 Bell Canyon Monitoring

Two wells in the monitoring network are completed in the Bell Canyon, DOE-2 to the north of the WIPP site and Cabin Baby (CB)-1 to the south (Figure HYDRO-1). These wells are monitored to evaluate whether oil and gas activities in the Bell Canyon are affecting the hydraulic head beneath the WIPP site. Water level elevations are plotted for the period of January 2018 through January 2025 in Figure HYDRO-25. Since 2018, water levels in DOE-2 have risen slowly but remained relatively stable. In contrast, CB-1 shows a steady increase of ~8 m (26 ft) since 2018, indicating a more pronounced long-term upward trend.

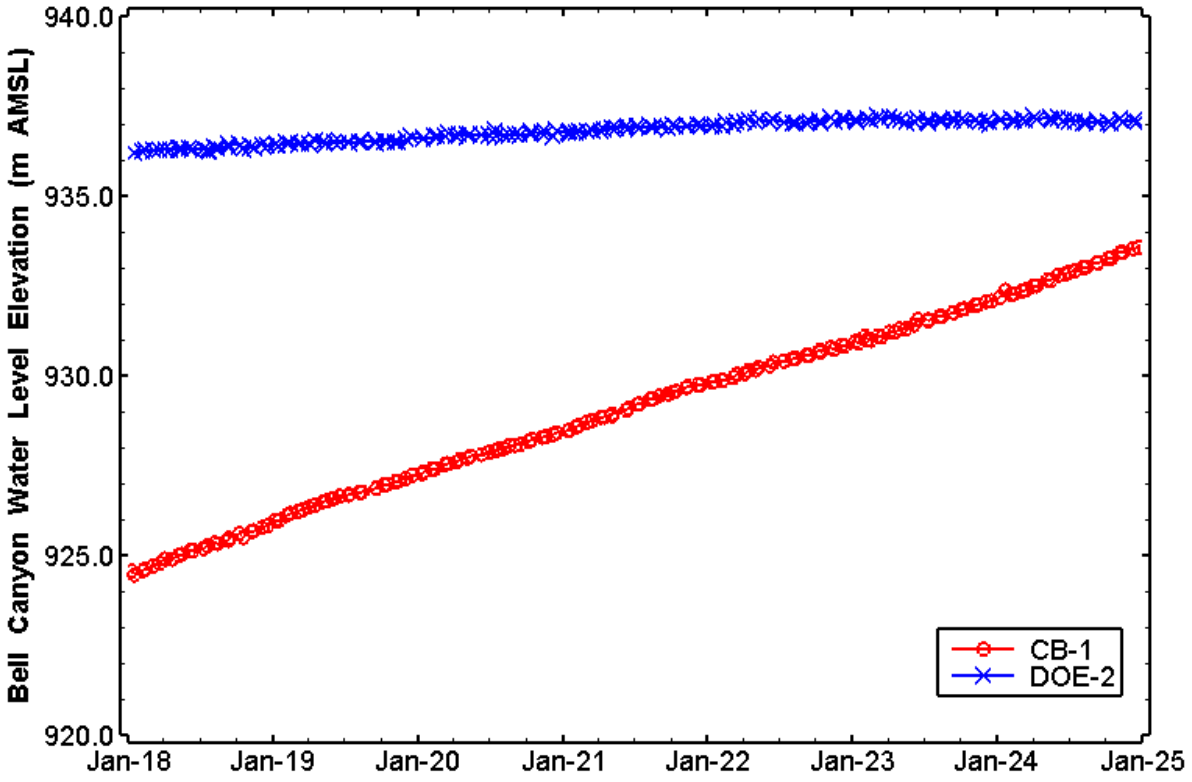


Figure HYDRO-25. Bell Canyon Water Levels

HYDRO-7.0 CULEBRA GROUND WATER FLOW DIRECTION

Change in Culebra flow pattern is one of the Compliance Monitoring Parameters (COMPs) used to meet 40 CFR 194.42 regulatory requirement. To detect changes in Culebra groundwater flow, a potentiometric map and particle travel time from the waste handling shaft to the WIPP LWB are derived every year. Further evaluation/analysis of data is triggered when the particle travel time falls outside the distribution found using 100 model runs used in the baseline PA (Kicker 2026). Using the average of the best 100 T-fields, as generated in Appendix TFIELD, Culebra groundwater flow model boundary conditions are optimized to match each year's observed equivalent freshwater heads (a representation of increased head value that accounts for the pressure exerted on the water column by dissolved solids). The contour maps for 2013 and 2023 are shown in Figures HYDRO-26 and HYDRO-27, respectively. A comparison of the freshwater head contours and particle paths is presented in Figure HYDRO-28.

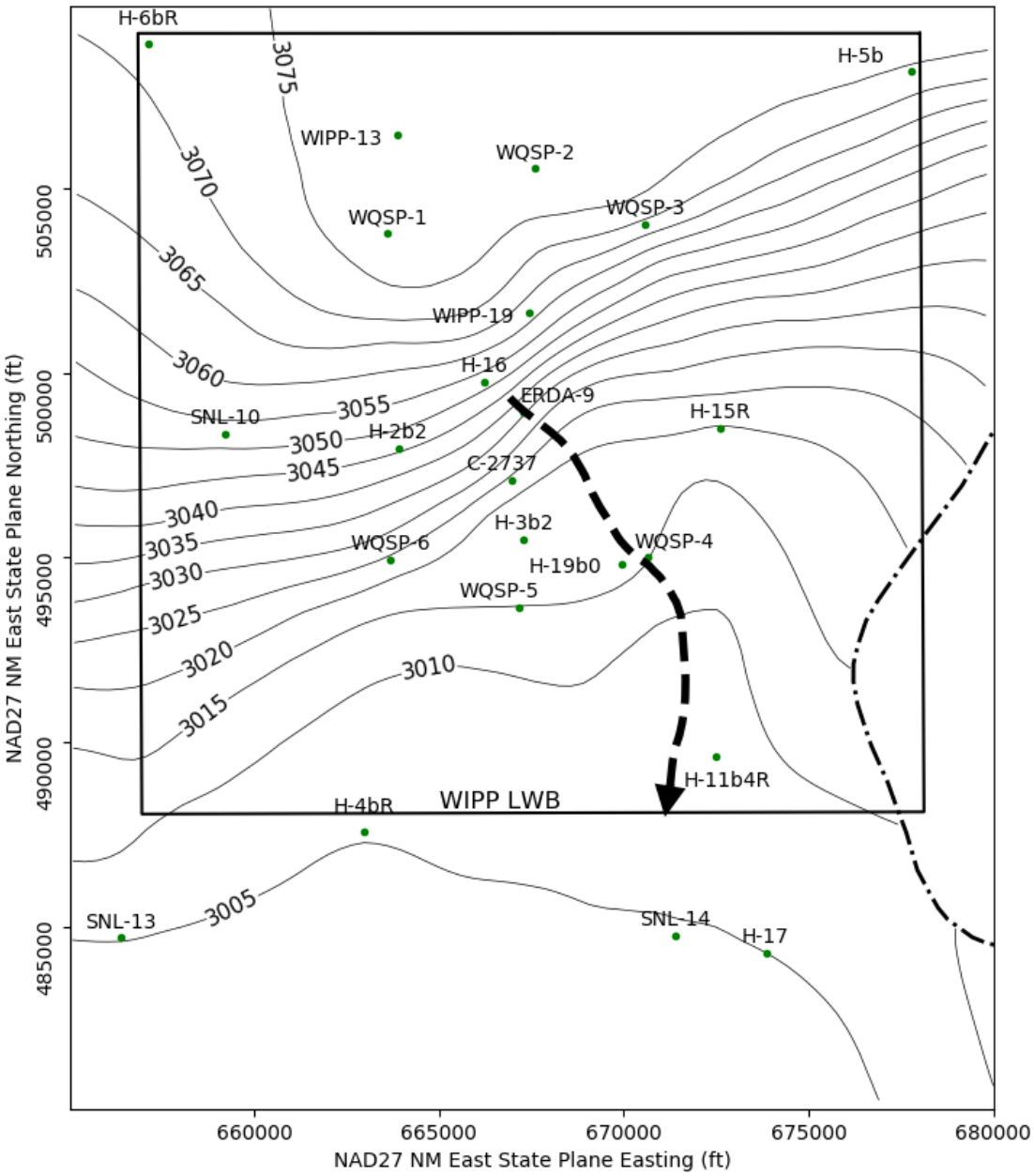


Figure HYDRO-26. 2013 Simulated Freshwater Head Contours (5-foot Contour Interval). The Dashed Line Represents the DTRKMF Simulated Particle Pathway from the Waste Handling Shaft to the WIPP LWB (Travel Time = 6,234 Years) (DOE 2014).

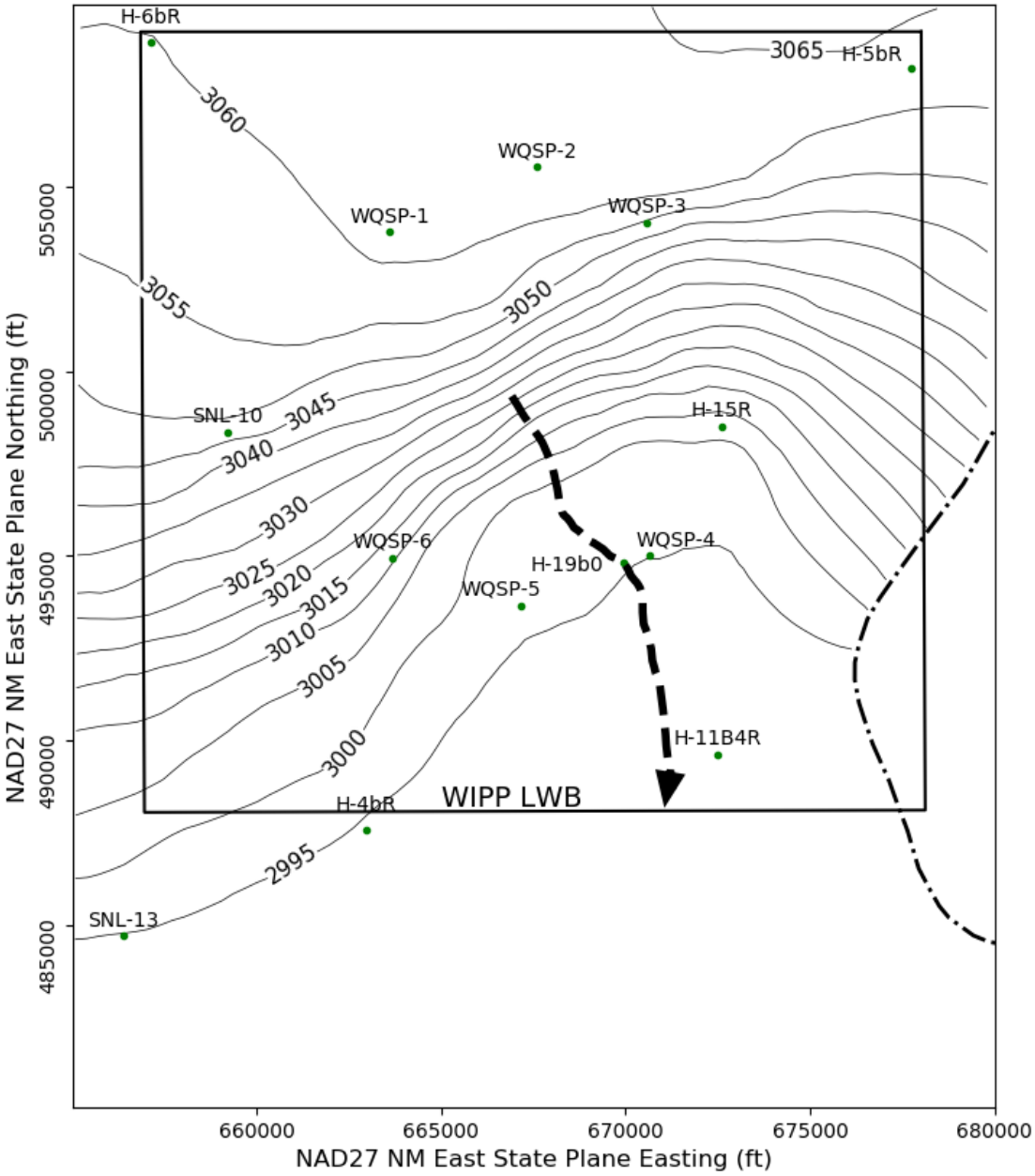


Figure HYDRO-27. 2023 Simulated Freshwater Head Contours (5-foot Contour Interval). The Dashed Line Represents the DTRKMF Simulated Particle Pathway from the Waste Handling Shaft to the WIPP LWB (Travel Time = 6,583 Years).

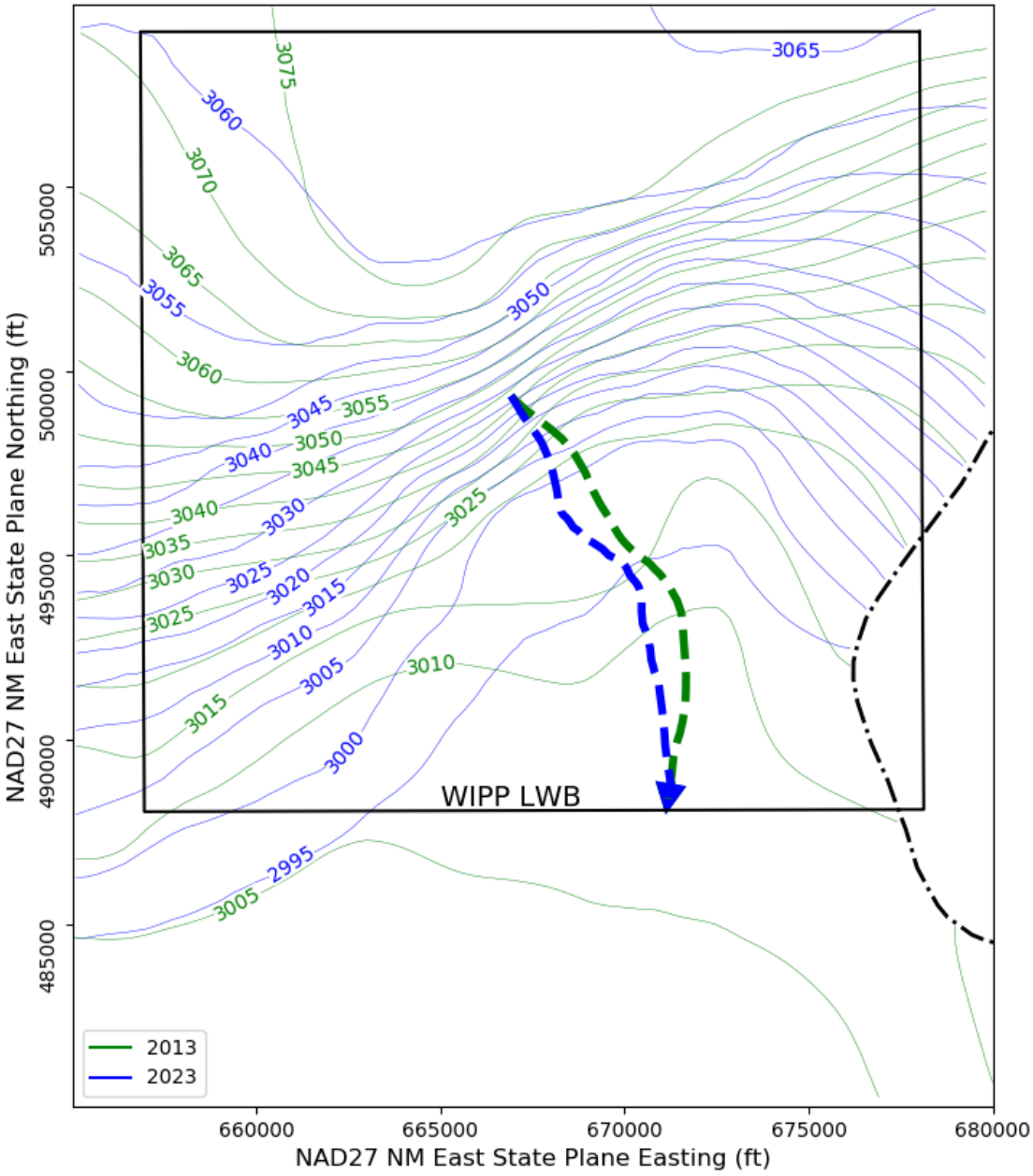


Figure HYDRO-28. Simulated Freshwater Head Contours for 2013 and 2023. From 2013 to 2023, there is a Decrease in Simulated Heads and a Westward Shift in Particle Path. These Changes are Due to a) the Use of New Calibrated Parameter Fields (Bowman et al. 2023) in 2023 and b) the Impact of Shaft 5 Mining on Culebra Water Levels.

HYDRO-8.0 SUMMARY

Three additional Culebra slug and pumping tests were analyzed to interpret transmissivity parameter estimates at one new and two replacement wells. The estimated Culebra *T* for well H-5bR had a geometric mean of 6.46E-08 m^2/s and mean *S* of 6.46E-08 differing from the previous test (*T* of 2.1E-07 m^2/s, *S* of 1.0E-05). The estimated Culebra T for WIPP-11R had a geometric mean of 7.59E-04 m2/s with a mean *S* of 3.19E-06 differing from the previous test (*T* of 4.27E-04 m^2/s, *S* of 6.40E-06). The new well (H-9bR) provided several diffusivity measurements for the portion of the aquifer south of the LWB.

Geochemical data have been collected from Culebra monitoring wells since 2017. Analysis of these samples corroborated several earlier geochemical interpretations and indicated that the expanded dataset may support refinement of parameterization within the Culebra flow model. Core hole C-3977 and the geological mapping of Shaft #5 provided additional geologic information, the lithology and stratigraphy that corroborates the reference stratigraphy derived from earlier shafts.

A combination of pressure and depth-to-water measurements are used to estimate fluid density in most Culebra wells at the WIPP. Equivalent freshwater heads, calculated from head measurements using these densities, are used in MODFLOW6 with an average of the 100 T-fields to a potentiometric surface map used to infer groundwater flow direction required for regulatory submittals. A comparison of the groundwater flow direction from CRA-2019 illustrates the changes in flow direction and release pathway.

The WIPP groundwater-monitoring program has continued to augment monthly manual water-level measurements in with high-frequency (15-min) pressure measurements using downhole pressure transducers. Water-level monitoring provides a general picture of the changes in hydraulic head occurring in the formations being monitored. Water levels are currently being monitored in the Culebra, Magenta, Dewey Lake, and Bell Canyon. Culebra water levels have generally stabilized post Mills Ranch pumping, with exception to those that are continually recovering or are in proximity to shaft leakage associated with Shaft 5 at the repository. Water levels in half of the Magenta wells were generally stable, again with exception of those that are near the shaft construction. The Dewey Lake water level was stable within a ~20-cm band since 2018. Bell Canyon water levels were stable in DOE-2 and rose steadily in CB-1 over the last decade.

HYDRO-9.0 REFERENCES

Akara, M. 2022. Analysis Report for AP-070: Analysis Report that Reviews and Re-analyzes Pumping Tests of the Western Monitoring Network. Carlsbad, NM: Sandia National Laboratories. ERMS 578338.

Akara, M. 2023. Analysis Report for Investigating Optimization Techniques to Determine Preferential Flow Direction in the Culebra. Carlsbad, NM: Sandia National Laboratories. ERMS 580833.

Akara, M. 2024. Analysis Report for Investigating Optimization Techniques to Determine Preferential Flow Direction in the Culebra [Milestone HYDRO-24-04], Carlsbad, NM: Sandia National Laboratories.

Barker, J. 1988. A generalized radial flow model for hydraulic tests in fractured rock, Water Resour. Res., 24(10), 1796-1804.

Beauheim, R. 2007. Diffusivity mapping of fracture interconnections. In Proceedings of the 2007 US EPA/NGWA Fractured Rock Conference. Westerville, OH, 2007. National Ground Water Association.

Beauheim, R. and R. Roberts. 1998. Flow-dimension analysis of hydraulic tests to characterize water-conducting features. Albuquerque, NM, and Livermore, CA: Sandia National Laboratories. SAND98-1927C.

Beauheim, R. and G. Ruskauff. 1998. Analysis of Hydraulic Tests of the Culebra and Magenta Dolomites and Dewey Lake Redbeds Conducted at the Waste Isolation Pilot Plant Site, Carlsbad, NM: Sandia National Laboratories. SAND98-0049.

Bourdet, D., J. Ayoub, and Y. Pirard. 1989. Use of pressure derivative in well-test interpretation, SPE Formation Eval. 4(2), 293-302.

Bowman, D. 2014. Analysis Report for AP-070: Analysis of the H-9bR Pumping Test Conducted From 8/6/12 to 8/22/12. Carlsbad, NM: Sandia National Laboratories. ERMS 562291.

Bowman, D. 2017. Analysis of the H-10cR Pumping Test Conducted from 7/24/17 to 7/27/17. Carlsbad, NM: Sandia National Laboratories. ERMS 568762.

Bowman, D. 2020a. Analysis Report for AP-070: Analysis of the H-15R Pumping Test Conducted From 1/19/09 to 1/22/09. Carlsbad, NM: Sandia National Laboratories. ERMS 573484.

Bowman, D. 2020b. Analysis Plan for Hydraulic-Test Interpretations, AP-070, Revision 3. Carlsbad, NM: Sandia National Laboratories. ERMS 574237.

Bowman, D. 2022a. Analysis Report for AP-070: Analysis of the H-5bR Slug Test Conducted On 12/7/21. Carlsbad, NM: Sandia National Laboratories. ERMS 577898.

Bowman, D. 2022b. Analysis Report for AP-070: Analysis of the WIPP-11R Pumping Test Conducted From 9/15/21 to 9/17/2021. Carlsbad, NM: Sandia National Laboratories. ERMS 578334.

Bowman, D. 2025. Analysis Report Comparing Newly Acquired Data versus the Conceptual Model. Carlsbad, NM: Sandia National Laboratories.*

Bowman, D., R. Kushnereit, M. Pedrazas, P. Johnson, N. Deeds, and J. Pinkard. 2023. Analysis Report Documenting the Data, Generation, and Calibration of T-fields for CRA-2024. Carlsbad, NM: Sandia National Laboratories. ERMS 579507.*

Bowman D. and R. Roberts. 2009. Analysis Report for AP-070, Analysis of Culebra and Magenta Hydraulic Tests Performed Between January 2005 and August 2008. Carlsbad, NM: Sandia National Laboratories. ERMS 550906

Burgess, A., T. Doe, T. Lowenstein, and J. Thies. 2008. Waste Isolation Pilot Plant Culebra Hydrogeologic Conceptual Model Peer Review Final Report. Carlsbad, NM: U.S. Department of Energy. ERMS 551513.

Dennehy, K., and J. Mercer. 1982. Results of hydrologic tests and water-chemistry analyses, wells H-5A, H-5B, and H-5C at the proposed Waste Isolation Pilot Plant site, southeastern New Mexico: U.S. Geological Survey Water-Resources Investigations 82-19.

Domski, P., and R. Beauheim. 2008. AP-125 Analysis Report: Evaluation of Culebra Brine Chemistry. Carlsbad, NM: Sandia National Laboratories. ERMS 549443.

Farinacci, M. and D. Bowman. 2022. Analysis Report Documenting Water Level Analysis, Revision 1, Analysis Report for AP-150, Analysis Plan for the Analysis of Observed Water Level Fluctuations. September 2022, Carlsbad, NM: Sandia National Laboratories. ERMS 578343.*

Farinacci, M., and P. Johnson. 2020. 2020 Calculated Densities. Carlsbad, NM: Sandia National Laboratories. ERMS 575042.

Farinacci, M., and P. Johnson. 2021. 2021 Calculated Densities. Carlsbad, NM: Sandia National Laboratories. ERMS 577068.

Farinacci, M., and P. Johnson. 2022. 2022 Calculated Densities. Carlsbad, NM: Sandia National Laboratories. ERMS 581035.

Hillesheim, M., L. Hillesheim, and N. Toll. 2007. Mapping of Pressure Head Responses of a Fractured Rock Aquifer to Rainfall Events. Carlsbad, NM: Sandia National Laboratories. ERMS 547326.

Holt, R. 1997. Conceptual Model for Transport Processes in the Culebra Dolomite Member, Rustler Formation. Albuquerque, NM: Sandia National Laboratories. SAND97-0194.

Holt, R., R. Beauheim, and D. Powers. 2005. Predicting Fractured Zones in the Culebra Dolomite. Albuquerque, NM: Sandia National Laboratories. SAND2005-4435 J.

Johnson, P. 2018. 2018 Calculated Densities. Carlsbad, NM: Sandia National Laboratories. ERMS 571445.

Johnson, P. 2019. 2019 Calculated Densities. Carlsbad, NM: Sandia National Laboratories. ERMS 572937.

Kicker, D. 2026. Specific Procedure SP 9-8: Monitoring Parameter Assessment Per 40 CFR 194.42. Revision 4. Carlsbad, NM: Sandia National Laboratories.

Kirkes, L. 2022. Analysis Plan AP-194: Analysis Plan to Evaluate and Analyze Current and Historical WIPP Groundwater Quality Data. Revision 0. Carlsbad, NM: Sandia National Laboratories. ERMS 577265.

Kirkes, L., M. Farinacci, M. Akara, and O. Lofton. 2022. Analysis Report for AP-194: Analysis Report for Evaluation and Analysis of Current and Historical WIPP Culebra Groundwater Quality Data, under Analysis Plan: AP-194 Rev.0. Carlsbad, NM: Sandia National Laboratories. ERMS 578504.

Kuhlman, K. 2010. Analysis Report, AP-111 Revision 1, Culebra Water Level Monitoring Network Design. Carlsbad, NM: Sandia National Laboratories. ERMS 554054.

Lofton, O. 2021. Milestone Report for WIPP Water Qualities Collected from 2019 to 2020 [Groundwater Sampling]. Carlsbad, NM: Sandia National Laboratories. ERMS 576354.

NOAA. 2025. National Oceanic and Atmospheric Administration: National Centers for Environmental Information. "WASTE ISOLT N PILOT PLANT" Metrological Station. 8/1/25. https://www.ncdc.noaa.gov/cdo-web/

Powers, D., A. Hall, J. Thurston, R. Holt, R. Salness, and B. Seal. 2019a. Basic Data Report for C-3976-4 (SSW2) for Waste Isolation Pilot Plant (WIPP) May 2019 (revised August 2019).*

Powers, D., R. Salness, B. Seal, A. Hall, J. Thurston, and R. Holt. 2019b. Basic Data Report for C-3976-1 (Dewey Lake 1) for Waste Isolation Pilot Plant (WIPP) March 2019 (revised August 2019).*

Powers, D., B. Seal, A. Hall, J. Thurston, R. Holt, and R. Salness. 2019c. Basic Data Report for C-3976-3 (Dewey Lake 2) for Waste Isolation Pilot Plant (WIPP) April 2019 (revised August 2019).*

Powers, D., J. Thurston, R. Holt, R. Salness, B. Seal, and A. Hall. 2019d. Basic Data Report for C-3976-2 (SSW1) for Waste Isolation Pilot Plant (WIPP) July 2019 (revised August 2019).*

Powers, D., R. Holt, R. Salness, B. Seal, A. Hall, and J. Thurston. 2018. Geology of C-3977 (Pre-shaft Corehole) for Waste Isolation Pilot Plant (WIPP). DOI:10.13140/RG.2.2.29086.84801.

Reyna, O. 2025. SP 9-11, Revision 4, Calculation of Densities for Groundwater in WIPP Wells. Carlsbad, NM: Sandia National Laboratories.

Reyna, O., and P. Johnson 2023. 2023 Calculated Densities. Carlsbad, NM: Sandia National Laboratories. ERMS 581106.

Reyna, O., and P. Johnson 2024. 2024 Calculated Densities [Dated 01/28/2025]. Carlsbad, NM: Sandia National Laboratories.

Roberts, R. 2006. Analysis of Culebra Pumping Tests Performed Between December 2003 and August 2005. Carlsbad, NM: Sandia National Laboratories. ERMS 543901.

Roberts, R. 2007. Analysis of Culebra Hydraulic Tests Performed Between June 2006 and September 2007. Carlsbad, NM: Sandia National Laboratories. ERMS 547418.

Salness, R. 2006. Basic Data Report for Well Plugging and Abandonment and Reconfiguration Activities for Fiscal Year 2005. Carlsbad, NM Field Office: U.S. Department of Energy. DOE/WIPP 05-3326.

Schuhen, M. 2010. Test Plan TP 03-01: Test Plan for Testing of Wells at the WIPP Site, Revision 3. Carlsbad, NM: Sandia National Laboratories. ERMS 553985.

Siegel, M., S. Lambert, and K. Robinson. 1991. Hydrogeochemical Studies of the Rustler Formation and Related Rocks in the Waste Isolation Pilot Plant Area, Southeastern New Mexico. Albuquerque, NM: Sandia National Laboratories. SAND88-0196.

Toll, N., and T. Rasmussen. 2007. Removal of barometric pressure effects and earth tides from observed water levels. Ground Water, 45(1), 101-105.

U.S. Department of Energy (DOE). 2014. Waste Isolation Pilot Plant Annual Site Environmental Report for 2013. Carlsbad, NM: U.S. Department of Energy. DOE/WIPP-19-3591.

U.S. DOE. 2019. Waste Isolation Pilot Plant Annual Site Environmental Report for 2018. Carlsbad, NM: U.S. Department of Energy. DOE/WIPP-19-3591.

U.S. DOE. 2020. Waste Isolation Pilot Plant Annual Site Environmental Report for 2019. Carlsbad, NM: U.S. Department of Energy. DOE/WIPP-20-3591.

U.S. DOE. 2021a. Basic Data Report for Well Plugging and Abandonment. Fiscal Year 2020. Carlsbad, NM: U.S. Department of Energy. DOE/WIPP-21-3626.

U.S. DOE. 2021b. Waste Isolation Pilot Plant Annual Site Environmental Report for 2020. Carlsbad, NM: U.S. Department of Energy. DOE/WIPP-21-3591.

U.S. DOE. 2022. Waste Isolation Pilot Plant Annual Site Environmental Report for 2021. Carlsbad, NM: U.S. Department of Energy. DOE/WIPP-22-3591.

U.S. DOE. 2023a. Waste Isolation Pilot Plant Annual Site Environmental Report for 2022. Carlsbad, NM: U.S. Department of Energy. DOE/WIPP-23-3591.

U.S. DOE. 2023b. Waste Isolation Pilot Plant Environmental Monitoring Plan. Carlsbad, NM: U.S. Department of Energy. DOE/WIPP-99-2194 Rev. 14.

U.S. DOE. 2024. Waste Isolation Pilot Plant Annual Site Environmental Report for 2023. Carlsbad, NM: U.S. Department of Energy. DOE/WIPP-24-3591.

U.S. DOE. 2025. Waste Isolation Pilot Plant Annual Site Environmental Report for 2024. Carlsbad, NM: U.S. Department of Energy. DOE/WIPP-25-3591.

U.S. Environmental Protection Agency. 1996. Environmental Protection Agency (EPA). 1996. 40 CFR Part 194: Criteria for the Certification and Recertification of the Waste Isolation Pilot Plant's Compliance with the 40 CFR Part 191 Disposal Regulations; Final Rule. Federal Register, vol. 61 (February 9, 1996): 5223–45.

Wu, C., X. Wu, C. Lu, Q. Sun, X. He, L. Yan, and T. Qin. 2021. Hydrogeochemical Characterization and its Seasonal Changes of Groundwater Based on Self-Organizing Maps. Water, 2021, 13, 3065.